



# HHS Public Access

Author manuscript

Cell Rep. Author manuscript; available in PMC 2022 February 24.

Published in final edited form as:

Cell Rep. 2022 January 18; 38(3): 110277. doi:10.1016/j.celrep.2021.110277.

## Tissue differences in the exosomal/small extracellular vesicle proteome and their potential as indicators of altered tissue metabolism

Ruben Garcia-Martin<sup>1,4</sup>, Bruna Brasil Brandao<sup>1,4</sup>, Thomas Thomou<sup>1,3</sup>, Emrah Altindis<sup>2,5,\*</sup>, C. Ronald Kahn<sup>1,5,6,\*</sup>

<sup>1</sup>Joslin Diabetes Center, Harvard Medical School, One Joslin Place, Boston, MA 02215, USA

<sup>2</sup>Boston College Biology Department, Higgins Hall, 140 Commonwealth Avenue, Chestnut Hill, MA 02476, USA

<sup>3</sup>Present address: Gryphon Technologies LC, 3811 Fairfax Drive, Arlington, VA 22203, USA

<sup>4</sup>These authors contributed equally

<sup>5</sup>These authors contributed equally

<sup>6</sup>Lead contact

### SUMMARY

Exosomes/small extracellular vesicles (sEVs) can serve as multifactorial mediators of cell-to-cell communication through their miRNA and protein cargo. Quantitative proteomic analysis of five cell lines representing metabolically important tissues reveals that each cell type has a unique sEV proteome. While classical sEV markers such as CD9/CD63/CD81 vary markedly in abundance, we identify six sEV markers (ENO1, GPI, HSPA5, YWHAB, CSF1R, and CNTN1) that are similarly abundant in sEVs of all cell types. In addition, each cell type has specific sEV markers. Using fat-specific Dicer-knockout mice with decreased white adipose tissue and increased brown adipose tissue, we show that these cell-type-specific markers can predict the changing origin of the serum sEVs. These results provide a valuable resource for understanding the sEV proteome of the cells and tissues important in metabolic homeostasis, identify unique sEV markers, and demonstrate how these markers can help in predicting the tissue of origin of serum sEVs.

### Graphical abstract

This is an open access article under the CC BY-NC-ND license.

\*Correspondence: altindis@bc.edu (E.A.), c.ronald.kahn@joslin.harvard.edu (C.R.K.).

#### AUTHOR CONTRIBUTIONS

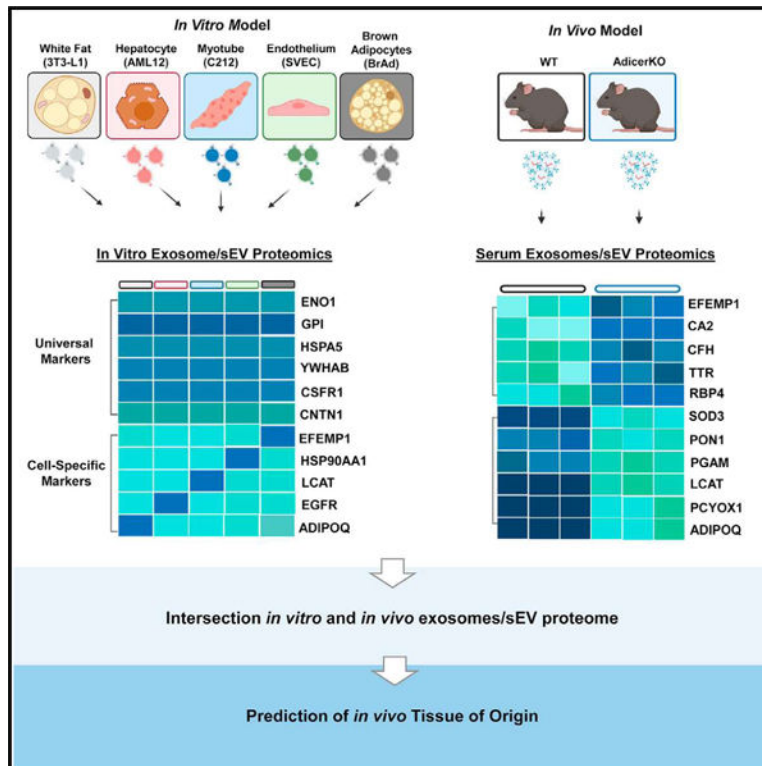
R.G.-M., B.B.B., and E.A. assisted with all of the *in vitro* experiments, proteomics analysis, and *in vivo* experiments. T.T. performed serum sEV isolation. All of the authors helped with the analysis of the data and writing the manuscript. E.A. and C.R.K. designed the research and supervised the project.

#### SUPPLEMENTAL INFORMATION

Supplemental information can be found online at <https://doi.org/10.1016/j.celrep.2021.110277>.

#### DECLARATION OF INTERESTS

The authors declare no competing interests.



## In brief

By performing comparative proteomics, Garcia-Martin et al. identify markers common to exosomes/sEVs from multiple cell types, as well as markers unique to each cell type. Using a lipodystrophy mouse model, they demonstrate the use of this sEV proteome dataset to predict the tissue of origin of circulating exosomes/sEVs *in vivo*.

## INTRODUCTION

Exosomes and other small extracellular vesicles (sEVs) have emerged as important mediators of cell-to-cell communication and metabolic regulation (Crewe et al., 2018; Thomou et al., 2017; Zhao et al., 2018). sEVs contain a wide range of molecules, including proteins, different subclasses of coding and non-coding RNAs, DNA, and several metabolites (Kalra et al., 2016; van Niel et al., 2018). sEVs are present in every fluid in the organism, including plasma/serum, urine, and cerebrospinal fluid. Because sEV cargo is influenced by physiological and pathological status, they can be used as markers for diagnosis and predicting the prognosis of a wide variety of diseases, including diabetes, obesity, cancer, and cardiovascular and neurodegenerative diseases (Hoshino et al., 2020; Kalluri and LeBleu, 2020; Mori et al., 2019). For example, sEVs in the circulation of obese patients have increased perilipin levels (Eguchi et al., 2016), whereas those from patients with Alzheimer's disease have higher levels of b-amyloid and phospho-tau protein (Rajendran et al., 2006; Saman et al., 2012). Tumor markers such as epidermal growth factor receptor variant III (EGFRvIII) and prostate-specific antigen have also been found increased

in serum sEVs from patients with glioblastoma or prostate cancer, respectively (Logozzi et al., 2017; Skog et al., 2008).

While work over the last decade has clearly established that the micro RNA (miRNA) cargo in sEV is regulated and cell type dependent (Garcia-Martin et al., 2021; Valadi et al., 2007; Wei et al., 2017), less attention has been paid to how protein sorting into sEVs may differ among different cell types (Angulski et al., 2017; Hoshino et al., 2015; Yoshioka et al., 2013). In the present study, we have used quantitative proteomics to compare the protein cargo of sEVs isolated from different cell lines representing the main tissues involved in metabolic disease, including white and brown adipocytes, muscle cells, hepatocytes, and endothelium, as well as differentiated murine stromal vascular fraction (SVF)-derived adipocytes. We show that while classic tetraspanin markers vary considerably in sEVs from different cell types, these metabolically important tissues release sEVs with similar levels of the metabolic enzymes enolase (ENO1) and glucose-6-phosphate isomerase (GPI), the chaperone HSPA5 (also known as BiP), the 14–3–3 protein beta/alpha (YWHA3), colony-stimulating factor receptor (CSF1R), and the GPI-anchored protein contactin-1 (CNTN1), which could be used as potential sEV markers. In addition, sEVs from each cell type contain unique proteins representing specific cell-type markers. Using this dataset, we can also predict the tissue of origin of some of the sEV proteins in serum samples. Thus, comparing sEVs from normal mice to mice with adipose tissue-specific Dicer knockout (AdicerKO), which have been shown to have enlarged brown adipose tissue (BAT) and decreased white adipose tissue (WAT) (Mori et al., 2014; Thomou et al., 2017), we found 25% of the proteins were significantly altered, including several that marked sEVs of white or brown adipocyte origin such as high-molecular-weight (HMW) adiponectin (ADIPOQ), which sits on the surface of the sEV membrane where it would be accessible to bind to its receptors in target cells. These data demonstrate the unique nature of the proteins in sEVs of different cell types and how levels of these could be used as biomarkers for the identification of the tissue of origin.

## RESULTS

### Cells produce widely varying levels of sEVs with distinct proteomes

To characterize and compare the sEV/exosomal protein cargo of the major metabolic tissues, we used five murine cell lines that are widely used as models of metabolic regulation: i.e., differentiated 3T3-L1 cells representing white adipocytes, immortalized differentiated brown adipocytes (BrAd), AML12 cells representing hepatocytes, differentiated C2C12 myotubes representing skeletal muscle, and SVEC representing endothelial cells. All cells were grown to confluence, differentiated when necessary (3T3-L1, BrAd, and C2C12 cells), and then put in medium supplemented with exosome-free fetal bovine serum. After 48 h, the sEVs/exosomes from each of the cell types were isolated using a standard ultracentrifugation (UC)-based method (They et al., 2006) (Figure 1A).

For all cell types, the obtained vesicles ranged in size between 50 and 200 nm, corresponding to exosome size, as measured by electron microscopy (Figure 1B). As we previously reported, the size distribution of the sEVs did not differ among the different cell types as measured by nanoparticle tracking analysis (Garcia-Martin et al., 2021). The

number of vesicles released by these cells into the culture medium over 48 h differed significantly among cell types. Differentiated 3T3-L1 white adipocytes released significantly more sEVs per cell than all other cell types, while differentiated C2C12 myotubes released the least (Figure 1C). Protein concentrations of the vesicles paralleled the number of vesicles released (Figure 1D). As the size of vesicles released from different cell lines did not differ, these data suggest that sEVs from different cellular origins contain a similar protein load but are released at different rates, with white adipocytes being the highest sEV producer and C2C12 the lowest, at least of the five cell types studied. This is consistent with our previous observation that adipose tissue is a major contributor of circulating exosomal miRNAs and that KO of the miRNA processing enzyme Dicer in adipose tissue causes a marked reduction in circulating exosomal miRNAs (Thomou et al., 2017).

### sEV protein cargo is different among cell types

To explore potential differences in the protein cargo among the sEVs released from these different cells, we subjected the isolated sEVs to tandem mass tag (TMT) labeling, followed by liquid chromatography/tandem mass spectrometry (LC-MS/MS)-based proteomics. In total, 431 proteins were identified, 349 of which were identified in at least 2 of 3 biological replicates (Table S1). Gene Ontology (GO) cellular component ontology of these proteins revealed that most of them were from the extracellular region (cell surface and secreted proteins), cytoplasm, and plasma membrane (Figure S1A). Functionally, there was enrichment for proteins involved in protein metabolism, macro-molecule processing, signal transduction, and the stress response (Figure S1B).

Principal-component analysis (PCA) of the 349 sEV proteins revealed that the 5 cell types fell into 2 main clusters, with myotubes (C2C12) and hepatocytes (AML12) forming one group and white adipocytes (3T3-L1), BrAd, and endothelial cells (SVEC) forming the second (Figure 2A). Consistent with the PCA analysis, we identified 63 proteins in the cluster shared by sEVs from AML12 hepatocytes and C2C12 myotubes, while there was a total of 49 proteins in the second cluster, with 13 proteins enriched in sEVs of both white adipocytes and BrAd, 25 proteins enriched in sEVs from BrAd and endothelial cells, and 11 proteins enriched in sEVs released by white adipocytes and BrAd and endothelial cells (Figures 2A–2C). In addition to these overlapping proteins, sEVs of each cell type showed some unique or highly enriched proteins compared to all of the other cell types, with 12 proteins uniquely enriched in 3T3-L1 sEVs, 19 proteins in AML12 sEVs, 67 proteins in C2C12 sEVs, 13 proteins in SVEC sEVs, and 17 in BrAd sEVs (Figures 2C and 2D; Table S1).

To determine possible functional links of the sEV proteins in each cell type, we performed pathway analysis. This revealed a similar bimodal clustering pattern. Thus, sEVs released by endothelial cells and white and brown adipocytes were enriched in proteins involved in catabolic processes and the metabolism of organic acids, carboxylic acids, and nitrogen compounds (Figure S1C). Strikingly, sEVs isolated from these cells by differential centrifugation also contained detectable levels of 10 of the 12 enzymes in the glycolytic pathway (Figures 3A and 3B). This finding was confirmed in sEVs isolated using an additional step of purification (i.e., size exclusion chromatography [SEC]) after differential

centrifugation (Figures S1D and S1E). In addition, sEVs from endothelial cells and brown and white adipocytes were enriched in important enzymes of fatty acid synthesis, such as ATP-citrate lyase (ACLY) and fatty acid synthase (FASN), and lipoprotein metabolism such as low-density lipoprotein receptor-related protein 1 (LRP1) (Figures S2A and S2B). In contrast, sEV proteins released by AML12 hepatocytes and C2C12 myotubes showed an enrichment in proteins involved in cell migration/adhesion, immune response, regulation of cellular architecture, and lipid and glycerophospholipid metabolism (Figure S1C). The latter cluster also contained multiple members of the serpin superfamily. Serpins are involved in a broad range of functions, including inhibition of immune cell-derived proteases (Serpina1b and a3k); transport of glucocorticoids, progesterin, and thyroxine (Serpina6 and a7); regulation of coagulation and fibrinolysis (Serpinc1, d1, and f2); and inhibition of complement (Serping1) (Law et al., 2006; Silverman et al., 2001) (Figure S2C). These data demonstrate that despite the remarkable differences among these metabolically important cell lines, there are unexpected similarities in sEV protein cargo, resulting in two clear patterns in these different cell types.

### Known and newly identified sEV markers differ among cell lines

Tetraspanins represent a conserved family of proteins involved in many different functions, including cell adhesion, motility, and proliferation, and are involved in sEV cargo selection and trafficking (Andreu and Yanez-Mo, 2014; Kowal et al., 2016). Previous studies have shown that tetraspanins such as CD63, CD9, and CD81 are enriched in the sEV proteome, and thus, these have often been used as markers for sEV identification, quantitation, or purification (Escola et al., 1998; French et al., 2017; Jeppesen et al., 2019; Kowal et al., 2016). However, our comparative proteomic analysis revealed that CD9, CD63, and CD81, the most commonly used markers of sEV, display very different levels in the sEV derived from different cell types. Thus, by quantitative LC/MS-MS, these three tetraspanins were very abundant in sEVs from hepatocytes and myotubes but were present at 5- to 20-fold lower levels in sEVs from endothelial cells and white and brown adipocytes (Figure 4A). These results were confirmed by immunoelectron microscopy, showing CD63 as being much more abundant in C2C12-derived sEVs than in SVEC-derived sEVs and by immunoblotting (Figures 4B and 4C). In addition, cellular proteins calnexin (CANX) and GM130, as well as mitochondrial CYC1 and TOMM20 were not detected in sEV samples (Table S1).

In contrast to the variable presence of the tetraspanins, we identified six proteins that were present at similar levels among the sEVs from all of the cell types that may serve as better markers of sEVs. These include the cytosolic enzymes ENO1 and GPI (Figure 3B), heat shock protein family A member 5 (HSPA5, also known as HSP70 or BiP), and YWHAB (Figure 4D). In addition, sEVs contain similar amounts of two membrane proteins, CNTN1 and CSF1R (Figure 4D). Whereas the first group of proteins and enzymes would be predicted to localize in the sEV lumen, the latter are categorized as membrane proteins, which could also serve as surface markers.

## Identification of cell-type-specific sEV markers

One of the main goals of the present study was to identify proteins specifically enriched in sEVs of individual cell types that could serve as tissue- or cell-type-specific markers. From our quantitative proteomics data, we identified 38 proteins that were highly enriched in sEVs from 3T3-L1 cells, and of these, 12 were 3T3-L1 specific. Similarly, 84 proteins were highly enriched in sEVs of AML12 cells, with 19 of these being AML12 specific; 137 proteins were detected in sEV of C2C12 cells, with 67 of these being C2C12 specific; 55 proteins were enriched in sEV of SVEC, with 13 being SVEC specific; and 69 proteins were enriched in sEVs from BrAd, with 17 being BrAd specific (Figures 2C, 2D, and S2D–S2H; Table S1).

The specific markers identified by proteomics in sEVs isolated from each of the five cell types can be confirmed by immunoblotting (Figure 5). Thus, proteomic analysis of sEVs derived from 3T3-L1 white adipocytes show enriched ADIPOQ and the fatty acid translocase CD36 compared to the other cell types, and this enrichment was confirmed by immunoblotting (Figures 5A, S3A, S4A, and S4B). More interesting, sEVs from AML12 hepatocytes were enriched with two plasma membrane receptors, EGFR and integrin beta-1 (ITGB1), in the proteomics analysis, and this was verified by immunoblotting (Figures 5B, S3B, S4C, and S4D). Western blot analysis also confirmed that C2C12-derived sEVs were enriched with secreted protein acidic and cysteine-rich (SPARC) and insulin growth factor-binding protein 5 (IGFBP5) (Figures 5C, S3C, S4E, and S4F), whereas SVEC were highly enriched with the important chaperone HSP90 (Figures 5D and S4G). Finally, both mass spectrometry (MS) and western blot analysis showed enrichment of periostin (POSTN) and thrombospondin-1 (THBS1) in BrAd sEVs (Figures 5E, S3D, S4H, and S4I). Thus, each cell type releases sEV with cell-type-specific markers, and these can be identified by both MS and western blotting.

The incorporation of proteins in sEVs may depend on abundance in a cell type or sorting into the pathway of exosomal secretion. Immunoblotting showed that some of the proteins found in sEVs were present in proportion to their levels in the cell, such as ADIPOQ (Figure 5A), SPARC (Figure 5C), FASN (Figure S2B), and IGFBP5 (Figure S3C). However, for other proteins such as ITGB1, HSP90, and POSTN, their abundance in sEVs released by some cell types was markedly elevated even compared to the cellular levels. For instance, ITGB1, an AML12-specific sEV marker (Figures 5B and S4C), displayed similar levels of expression in AML12, C2C12, and SVEC cell bodies, but a high level of this protein only in sEVs derived from AML12 cells (Figure 5B), indicating the existence of a hepatocyte-specific sorting mechanism for ITGB1 into sEVs. Likewise, POSTN was highly enriched only in sEVs from BrAd, although 3T3-L1, AML12, SVEC, and BrAd cells showed comparable levels of this protein in their cell bodies, and C2C12 cells had an even higher cellular content, but little in its sEV (Figures 5E and S4H). Thus, BrAd must have a cell-specific sorting mechanism to direct POSTN into its released vesicles that is absent in these other cell types.

To determine whether the sEV proteome of these cultured cell models was similar to their primary cell counterparts, we isolated the SVF from the subcutaneous inguinal WAT (sWAT) depots of wild-type (WT) mice, differentiated these cells into adipocytes, and isolated their

released sEVs by differential centrifugation in parallel with sEVs from differentiated 3T3-L1 white adipocytes. We subjected the sEVs derived from both cell models to MS proteomic analysis. A very strong correlation in the sEV proteome of 3T3-L1 and SVF-derived adipocytes was observed ( $r^2 = 0.7195$ ; Figure S5A; Table S2). Several previously identified 3T3-L1-specific sEV markers (CD36, FABP4, COL6A3, and CAV1) were found enriched in sEVs released by SVF-derived adipocytes and depleted in hepatocyte models (AML12 and primary hepatocytes) (Figure S5B). These data indicate that the exosomal/sEV proteome released by 3T3-L1 cells, the widely used *in vitro* model for adipocytes, closely resembles the exosomal/sEV proteome of SVF-derived adipocytes, in line with previous observations (Durcin et al., 2017).

Moreover, we compared the reproducibility of the sEV proteome obtained by differential centrifugation with the proteome of sEV isolated using an additional step of purification, namely SEC. To this end, we isolated sEVs from differentiated 3T3-L1 adipocytes and AML12 cells with the differential centrifugation protocol used for our previous experiments (here labeled sEV-p100). An aliquot of these samples was subjected to SEC, and the flow-through was collected in 30 fractions (Figure S6A). Fractions 7–10 were enriched in small vesicles as measured by nanoparticle tracking analysis (NTA), showed a peak of protein concentration and were positive for classical sEV markers CD63 and CD9 (Figure S6B–S6D). These further purified vesicles were labeled sEV-SEC. For comparison, we also collected fractions 17–24, which showed a peak of protein concentration, but showed no vesicles as accessed by NTA and were depleted from sEV markers by Western blot analysis (Figures S6B–S6D). Comparison of the proteome of the sEV isolated by differential centrifugation (sEV-p100) and the sEV isolated by differential centrifugation plus SEC (sEV-SEC) showed a very strong correlation in the identity and abundance of the proteins. This was true for both 3T3-L1 sEV ( $r^2 = 0.9481$ ) and AML12 sEV ( $r^2 = 0.7544$ ) (Figures S6E and S6F; Table S2). These data indicate that sEV isolated by UC alone, as was used for the 5 cell types (i.e., 3T3-L1, AML12, C2C12, SVEC and BrAd), show a similar and high level of purity as sEV purified by SEC and are largely depleted from contaminants such as large protein complexes or lipoproteins.

### Serum sEV proteins as indicators for tissue alterations in metabolic disease

We have previously shown that adipose tissue is a major contributor for the pool of serum miRNAs in exosomes/sEVs such that fat-specific AdicerKO, the endoribonuclease responsible for miRNA maturation, leads to a marked downregulation of almost half of the miRNAs found in serum exosomes/sEVs (Thomou et al., 2017). The AdicerKO mouse also exhibits severe lipodystrophy of WAT, enlargement and altered morphology of BAT, and multiple metabolic abnormalities, including marked reduction in serum adiponectin, increased levels of FGF-21, marked glucose intolerance, and insulin resistance (Mori et al., 2014; Thomou et al., 2017). Some components of this phenotype, such as the increased FGF-21, could be attributed directly to the reduction in circulating exosomal miRNAs, since replacement of some of these miRNAs returned FGF-21 levels toward normal. To determine whether sEV protein cargo was also altered and may contribute to the metabolic phenotype, we isolated serum sEV from 12-week-old control and AdicerKO mice and subjected them to comparative proteomics (Figure 6A).

A total of 349 proteins were reproducibly identified in sEVs of at least two-thirds of samples. Of these, 86 (24.6%) were differently expressed between control and KO mice, with 40 upregulated and 46 downregulated in AdicerKO versus control sEVs (false discovery rate [FDR] < 0.05) (Figure 6B; Table S3). Enrichment and GO categorical analysis revealed that among the top 10 upregulated pathways represented by the differentially abundant proteins were pathways involved in retinol metabolism and complement activation, including significantly altered levels of retinol binding 4 (RBP4), transthyretin (TTR), and complement factors H (CFH) and 3, 5, 7, and 9 (C3/5/7 and -9) (Figures 6C and 6D; Table S3). By contrast, among the downregulated proteins, the top 10 processes identified were the inflammatory response and iron metabolism, with significant decreases in serum amyloid p-component (APCS), serum amyloid A protein (SAA1) and C1 esterase inhibitor (Serping1), ceruloplasmin (CP), haptoglobin (HP), hemopexin (HPX), and extracellular superoxide dismutase [Cu-Zn] SOD3 (Figures 6E and 6F; Table S3). Interestingly, the highly changed proteins included proteins normally secreted by the liver, as well as adipose and other tissues (Arner et al., 2014; Maffei et al., 2016; Smith and Kahn, 2016).

In an attempt to track the likely tissue of origin of the significant altered proteins in AdicerKO sEV, we intersected each of these proteins with the *in vitro* data on the cell-type-specific sEV proteins identified above. Using this approach, three of the proteins changed in serum sEV of AdicerKO mice were predicted to be from hepatocytes (i.e., they were highly abundant or uniquely detected in sEV from AML12 cells), and all of these were increased in sEVs from AdicerKO mice (Figures S7A and S7B). Only one protein was predicted to be derived from SVEC (complement factor C3), and this was also upregulated in the AdicerKO mice (Figures S7A and S7B). However, 25 proteins were predicted to be derived from muscle cells, based on the high abundance in sEVs from C2C12 cells, 12 of which were upregulated and 13 were downregulated (Figures S7A and S7B). Most important, five proteins were predicted to be adipocyte specific. Of these, all of the sEV proteins predicted to be from white adipocytes, including the glycolytic protein phosphoglycerate mutase (PGAM1), the protease inhibitor Serpina10, prenylcysteine oxidase-like (PCYOX1) and the adipokine ADIPOQ, were decreased in serum sEVs from AdicerKO mice. In contrast, EFEMP1 (EGF-containing fibulin-like extracellular matrix protein 1, also called fibulin-3), which is unique to BrAd sEVs, was increased (Figures 7A and 7B). These changes are consistent with the marked decrease in WAT and increase in BAT observed in these mice. Western blotting confirmed a significant decrease in PGAM1 specifically in sWAT of AdicerKO mice, with no change in BAT, liver, and muscle. Moreover, a slight but not significant increase in EFEMP1/fibulin-3 protein in the BAT of AdicerKO mice was also observed, while its expression was decreased in liver and unchanged in the sWAT or skeletal muscle of AdicerKO mice (Figures 7C, 7D, S7C, S7D, and S7F). These data suggest that changes in the abundance of proteins in serum sEVs can reflect changes in tissue mass and protein expression in the tissue that selectively export these proteins into their sEV.

### Adiponectin as a marker of sEVs from white adipocytes

We further explored the adipokine ADIPOQ since it is an important insulin sensitizer, is known to be secreted uniquely from adipocytes (Ouchi et al., 2011), and serves as a unique

marker of white adipocyte sEVs. ADIPOQ is a 244-amino acid polypeptide that exists in the circulation in three oligomeric complexes: a low-molecular-weight (LMW) trimer of ~70 kDa, a medium-molecular-weight (MMW) hexamer of ~140 kDa, and an HMW oligomer of ~300 kDa containing at least 18 monomers (Peake et al., 2005; Shapiro and Scherer, 1998). HMW adiponectin is the major bioactive form and, when bound to its receptors AdipoR1/2, activates AMP-activated protein kinase (AMPK) or peroxisome proliferator-activated receptor gamma (PPAR $\gamma$ ) pathway in a tissue-dependent manner (Yamauchi and Kadowaki, 2013; Zhou et al., 2009). In addition, HMW adiponectin binds to T-cadherin in endothelial cells, regulates vascularization (Parker-Duffen et al., 2013), and has been shown to stimulate sEV release (Obata et al., 2018).

Immunogold staining confirmed the presence of ADIPOQ in sEVs (Figure 7E). Enzyme-linked immunosorbent assay (ELISA) and western blot analysis of serum before and after sEV isolation revealed that most of the ADIPOQ in serum is free and that only a small fraction is present in sEV fractions, with the MMW and HMW forms being the most abundant forms in both fractions (Figures 7F and 7G). In AdicerKO mice, there was a decrease in the abundance of both forms in serum and sEV (Figures 7F and 7G). This possibly occurred due to the lipodystrophy observed in the KO group, considering that ADIPOQ protein expression in sWAT of both control and AdicerKO mice was similar (Figures S7E and S7F). To determine whether ADIPOQ in sEV was on the surface or in the lumen of the vesicle, we treated sEVs with proteinase K both before and after disruption of the vesicular membrane with Triton X-100. We found that proteinase K was able to digest the ADIPOQ associated with sEVs both before and after the addition of the detergent (Figure 7H). Thus, ADIPOQ is a unique marker of sEVs from white adipocytes localized on the outer membrane of these sEVs, and therefore has the potential to bind to the ADIPOQ receptors (e.g., AdipoRs, T-cadherin) and affect the targeting of these exosomes/sEVs.

## DISCUSSION

Exosomes and other sEVs represent an important means of transport of molecules and information between cells of the body (Crewe et al., 2018; Thomou et al., 2017; Ying et al., 2017). These informational molecules include miRNAs, DNAs, and proteins. Here, we have applied quantitative proteomics to characterize the proteins of the exosomes/sEVs released by five different cell types that play major roles in the regulation of systemic metabolism (white and brown adipocytes, hepatocytes, myotubes, and endothelial cells) and used this dataset to predict the tissue of origin of serum sEV proteins in a lipodystrophic insulin-resistant mouse model.

We found that although there are common or shared proteins among sEVs, each of these five cell types releases sEVs containing unique or almost unique proteins that could be identified by MS and confirmed by immunoblotting. sEVs released by 3T3-L1 white adipocytes contain 12 unique proteins, including ADIPOQ and CD36; sEV from AML12 hepatocytes had 19, including ITGB1 (CD29) and EGFR; sEV from C2C12 myotubes had 67, including SPARC and IGFBP-5; sEVs from endothelial cells had 13, including HSP90; and sEVs from BrAd had 17, including POSTN and THBS1. For some of these, such as ADIPOQ, the unique presence of the protein in the sEVs reflected the unique presence

in the cell. In several cases, the relatively high level of the protein in the sEV was not due to unique or high expression in the cell but to selective sorting of the protein by the cell for exosomal export. For example, ITGB1/CD29, which serves as a cell surface receptor for integrin  $\alpha 1/\alpha 2$ , was present in the cell bodies of many of the cell types studied but was highly abundant only in the sEVs from AML12 hepatocytes, indicating a more effective sorting of this protein into sEVs in hepatocytes compared to the other cell types. Likewise, POSTN, which functions as a ligand for  $\alpha V/\beta 3$  and  $\alpha V/\beta 5$  integrins and is involved in the adhesion and migration of epithelial cells, is expressed in multiple cell types but more efficiently packaged in the sEVs from BrAd than other cells. These data suggest that the packaging mechanism is selective, not only for the protein to be sorted but also for the secreting cell type. Selective sorting may be functionally important since several of these proteins can serve as receptors or ligands for cell surface receptors, thus serving to target the sEVs to specific cell types that have the complementary protein on their surface. Protein cargo selection is a complex process that involves different components of the endosomal route and the plasma membrane, such as endosomal sorting complexes required for transport (ESCRT) proteins, lectins, syntenin, syndecans, tetraspanins, and even the specific lipid composition of the plasma membrane (Mathieu et al., 2019; Villarroya-Beltri et al., 2014). Exactly how certain proteins are more efficiently sorted than others and how this is regulated in a cell-type-specific manner remains unknown, although post-translational protein modification, level of polymerization of the protein, and their interactions with members of the endosomal route may favor its selection into the exosomes (Moreno-Gonzalo et al., 2014; Yang and Gould, 2013).

One surprising finding of this study is that the “classical” markers of sEV, the tetraspanins CD9, CD63, and CD81, are not equally abundant in sEVs from all cell types. While sEVs from muscle have high levels of all three tetraspanins, sEVs from AML12 liver cells were rich in only CD9 and CD81, and the other three cell types had low levels of all three tetraspanins. Similar differences in tetraspanin markers have been observed for sEV-released multiple cell lines (Kugeratski et al., 2021; Saunderson et al., 2008). By contrast, we could identify six proteins that were almost equally abundant in the sEVs of all five cell types: two glycolytic enzymes (ENO1, GPI), two protein-binding proteins (HSPA5 and YWHAB), and two membrane proteins (CSF1R and CNTN1). The latter proteins could represent a novel signature of sEVs. The latter two proteins could also play a role in the docking of the sEV to target cells or the uptake of sEVs from serum, since they would be predicted to reside in the membrane of the vesicle.

In addition to the proteins that were unique to each cell type or common to all cell types, we were able to identify two main types of sEVs based on overlapping protein cargo. Hepatocytes and myotubes formed one cluster, while endothelium and white and brown adipocytes formed the second. Considering the very different complement of proteins in these diverse cell types, the finding of these similarities in the protein content of these two clusters suggests some conserved protein sorting mechanisms among these two groups. Almost 20% (63 of 349) of proteins were common between sEVs from hepatocytes and myotubes, despite the large differences in the protein repertoire of these cells (Wu et al., 1994; Yaffe and Saxel, 1977). Among the common proteins for this cluster were multiple members of the serpin superfamily that have a wide range of functions, including

the inhibition of immune cell-derived proteases (Serpina1, -b, and -3k); the transport of glucocorticoids, progesterin, and thyroxine (Serpina6 and 7); the regulation of coagulation and fibrinolysis (Serpinc1, -d1, and -f2), and the inhibition of complement activation (Serping1) (Law et al., 2006; Silverman et al., 2001). The presence of these serpins in sEVs from muscle and liver suggests a role for these sEVs in the regulation of some of these functions.

The sEVs of endothelial cells and white and brown adipocytes formed the second cluster and shared 11 proteins that were highly enriched. There were 25 additional proteins shared by the sEVs of endothelial cells and BrAd and 13 shared by sEVs from brown and white adipocytes. Among the proteins in this second cluster, several enzymes involved in carbohydrate metabolism (phosphoglycerate kinase 1 [PGK1], pyruvate kinase isoforms M1/M2 [PKM], and lactate dehydrogenase B [LDHB]) or the synthesis of fatty acids (ACLY and FASN) were identified. Previous studies have shown that EVs can transfer enzymes from one cell type to another and promote the activity of metabolic pathway in the target cell (Gabriel et al., 2013; Sano et al., 2014; Yoshida et al., 2019; Zhang et al., 2019), and our data suggest that this may be especially important for sEVs from endothelial cells and adipocytes.

Identification of proteins that could specifically mark the tissue of origin of circulating sEVs could be useful in the management and diagnosis of diseases associated with altered exosomal/sEV profiles, such as various types of cancer, Alzheimer's disease, or metabolic diseases (Eguchi et al., 2016; Logozzi et al., 2017; Mariscal et al., 2016; Rajendran et al., 2006; Saman et al., 2012; Skog et al., 2008). To explore this possibility, we studied serum sEVs from AdicerKO. Phenotypically, these mice show a marked loss of WAT, enlargement and whitening of BAT, insulin resistance and glucose intolerance, and a massive reduction in circulating sEV miRNAs (Thomou et al., 2017). In the present study, we show that there is also a change in the proteome of the circulating sEV, and based on the specific proteins altered, it appears that both white and brown adipose depots, as well as other tissues, contribute to these differences. The fact that the 3T3-L1-derived sEV proteome paralleled closely the proteome of sEV released from differentiated SVF-derived adipocytes supports the idea of using *in vitro* cell lines as models for the tissue of origin of sEV *in vivo*. Thus, four proteins present in circulating sEV (ADIPOQ, PGAM1, Serpina10, and PCYOX1) are predicted to represent white fat based on our *in vitro* analysis, and all of them were decreased in serum sEVs. Conversely, the one protein predicted to represent sEVs from BrAd, EFEMP1/fibulin-3, was increased.

Other changes in the serum sEV proteome are more complex. For instance, RBP4 is produced mainly, but not exclusively, in the liver (Norseen et al., 2012) and was highly abundant in sEVs from AML12 and C2C12 in the cell-specific proteomic analysis. It is also increased in the sEVs isolated from the serum of the AdicerKO mice. RBP4 has been shown to be elevated in the circulation in insulin-resistant states and contributes to glucose intolerance (Yang et al., 2005). A study by Deng et al. (2009) found that adipose tissue from obese mice secrete sEVs containing high levels of RBP4, which are capable of inducing interleukin-6 (IL-6) production in macrophages. High-fat-fed AdicerKO mice exhibit slightly increased levels of circulating IL-6 (Mori et al., 2014). Thus, the increase in RBP4 in circulating sEVs could come from hepatocytes or white adipocyte fat and

contribute to the metabolic phenotype. In addition, many complement proteins, including CFH and C3/5/7 and 9, are also upregulated in circulating sEVs of AdicerKO mice. Increased levels of complement proteins have been previously observed in obesity, insulin resistance, and type 2 diabetes mellitus (Figueredo et al., 1993; Phielers et al., 2013a, 2013b; Shim et al., 2020); however, how many of these proteins are free or in sEVs in serum is unclear. By contrast, serum sEVs in AdicerKO mice have a downregulation of proteins that are important for oxidative metabolism and iron metabolism. Iron is essential for a variety of metabolic enzymes of oxygen metabolism (e.g., oxidases, peroxidase, catalases), electron transfer (cytochromes), and reactions involved in energy metabolism and DNA synthesis (Ponka, 1999).

One striking finding of this study is the high representation of almost all of the enzymes involved in the glycolytic pathway in sEVs, especially those from white and brown adipocytes. The presence of these enzymes in sEVs has been debated. While some studies, like ours, have found multiple glycolytic enzymes in circulating sEVs (in this case, in the context of exercise) (Whitham et al., 2018), others have suggested that they are contaminants present in sEV preparation isolated using a differential UC protocol (Jeppesen et al., 2019). In our study, not only were these glycolytic enzymes detected by MS-based proteomics and western blotting but we also found them in 3T3-L1-derived sEVs isolated by UC and UC combined with SEC, suggesting that their presence in sEVs is not simply contamination. To what extent these adipose adipocyte-derived proteins play roles in metabolic crosstalk will require further study; however, PGAM1, which regulates step 8 of glycolysis (Hitosugi et al., 2012), is significantly downregulated in circulating sEVs of AdicerKO mice.

The insulin sensitizer ADIPOQ is also downregulated in circulating sEVs in AdicerKO mice. Interestingly, the predominant form of ADIPOQ in sEVs is the HMW form, which is the most biologically active form (Pajvani et al., 2004). Based on protease sensitivity, this ADIPOQ is localized on the outer membrane of the sEV, indicating that it could bind to its receptors AdipoR1/2 or T-cadherin, leading to AMPK activation (Yamauchi and Kadowaki, 2013) or stimulation of endocytosis, followed by vesicle internalization and cargo delivery (Obata et al., 2018).

In summary, comparison of sEV proteins of five cell types representing the major tissues involved in diabetes, obesity, and the metabolic syndrome reveals that sEVs from each cell contain both unique and common proteins, with some of the latter being common to phenotypically and functionally different cell types, such as hepatocytes and myotubes or endothelium and white and brown adipocytes, indicating highly regulated sorting mechanisms present in each cell type. Importantly, the classical sEV markers (i.e., the tetraspanins) show very different levels in the sEVs of these five cell types, making them poor markers for the sEVs of these tissues. However, we have identified a set of proteins homogeneously released in sEVs of all of the cell types examined, which may prove to be more suitable sEV markers for metabolic disease. Finally, we demonstrate that by using markers identified in the *in vitro* data, we can predict the origin of sEV proteins in body fluids and how these change in metabolic disease. This could help to improve disease treatment by creating innovative methods to target only the affected tissue, thus avoiding possible side effects in healthy organs.

## Limitations of the study

Although we have confirmed that for cells in culture, sequential UC provides an exosomal/sEV isolate of similar purity to that obtained using an additional purification step of SEC, we cannot exclude the possibility that traces of abundant circulating proteins and lipoproteins could co-purify with sEV derived from serum samples. The relatively small amount of serum that can be obtained from a mouse (350–400  $\mu$ L), together with the loss of sEVs in each purification step, however, limits the application of combined isolation techniques for murine studies. In addition, in the present study, we have shown that ADIPOQ is present in/on the surface of white adipocyte-derived exosomes/sEVs. While the primary source of ADIPOQ is adipose tissue, as demonstrated by our work and multiple studies using ADIPOQ promoter to drive the expression of genes specifically in adipocytes (Brandao et al., 2020; Crewe et al., 2018; Eguchi et al., 2011; Mori et al., 2014), we cannot exclude the possibility that some circulating ADIPOQ is adsorbed from serum to the surface of sEVs derived from other cell types. However, this is likely to be very minor compared to the direct release of ADIPOQ in white adipocyte-derived sEVs.

## STAR★METHODS

### RESOURCE AVAILABILITY

**Lead contact**—Further information and requests for resources should be directed to and will be fulfilled by the lead contact, C. Ronald Kahn (c.ronald.kahn@joslin.harvard.edu).

**Materials availability**—This study did not generate new unique reagents.

### Data and code availability

- The mass spectrometry proteomics data have been deposited to the ProteomeXchange Consortium via the PRIDE partner repository with the dataset identifier PXD030240.
- This paper does not report original code.
- Any additional information required to reanalyze the data reported in this paper is available from the lead contact upon request.

### EXPERIMENTAL MODEL AND SUBJECT DETAILS

**Mice**—Control (AdipoQ-Cre<sup>-</sup> Dicer<sup>fl/fl</sup>) and AdicerKO (AdipoQ-Cre<sup>+</sup> Dicer<sup>fl/fl</sup>) (Mori et al., 2014) were males and 12 weeks of age in C57Bl/6J background. Mice were maintained at a 12-hr light-dark cycle with *ad libitum* access to tap water and normal chow diet (Mouse Diet 9F; PharmaServ). At sacrifice, serum and tissues were collected, snap-frozen in liquid nitrogen, and stored at  $-80^{\circ}\text{C}$ . Wild-type 8–10 week-old C57Bl/6J male mice (Jackson mice 00664) were used for isolation of preadipocytes (stromal vascular fraction of inguinal fat pad) and primary hepatocytes as described below. All animal experiments were conducted in accordance with institutionally review board (IRB) approved protocols.

**Cell culture**—3T3-L1 cells (ATCC, catalog nr CL-173, male genotype) were grown in growth medium [DMEM-high glucose (Thermofisher) supplemented with 10% fetal bovine

serum (Atlas Biologicals), 1% penicillin/streptomycin (Thermofisher) and 0.2% normocin (Invivogen). For all experiments, cells were grown to full confluence and differentiated using a differentiation cocktail containing 0.5 mM IBMX, 5 µg/mL insulin and 0.25 µM dexamethasone in growth medium for 3 days. Thereafter, cells were maintained in growth medium only supplemented with 5 g/ml insulin for 8 additional days. Brown pre-adipocytes (BrAd, male genotype) were generated as described previously (Fasshauer et al., 2000) and grown in DMEM-high glucose, 20% fetal bovine serum, 1% penicillin/streptomycin and 0.2% normocin. For the experiments, cells were grown to full confluence and differentiated by supplementing growth medium with 0.5 mM IBMX, 0.125 mM indomethacin, 1 µM dexamethasone, 20 nM insulin, 1 µM rosiglitazone and 1 nM T3 for 2 days. After that, cells were grown in culture medium supplemented with 20 nM insulin and 1 nM T3 for 9 more days. AML12 hepatocytes were purchased from ATCC (catalog nr CRL-2254, male genotype) and grown in DMEM/F12 high glucose, 10% fetal bovine serum, 1% penicillin/streptomycin and 0.2% normocin supplemented with insulin-transferrin-selenium-sodium pyruvate mixture (ITS-A, Thermofisher), 2.5 mM L-glutamine (Thermofisher), 15 mM HEPES (Millipore-Sigma) and 40 ng/ml dexamethasone. SVEC endothelial cells and C2C12 myoblasts were purchased from ATCC (catalog # CRL-2181, male; and CRL-1772, female, respectively) and cultured in the same growth medium as 3T3-L1 adipocytes. Upon confluence, C2C12 myoblasts were differentiated by culturing the cells in DMEM-high glucose supplemented with 2% horse serum, 1% penicillin/streptomycin and 0.2% normocin for six additional days. All reagents above were purchased from Millipore-Sigma unless otherwise stated.

## METHOD DETAILS

**Stromal vascular fraction (SVF) isolation and adipocyte differentiation**—Wild-type C57Bl/6J male mice (8–10 weeks old) were anesthetized with avertin. Subcutaneous inguinal adipose tissue (sWAT) was collected and further digested in isolation buffer (123 mM NaCl, 5 mM KCl, 1.3 mM CaCl<sub>2</sub>, 5 mM Glucose, 100 mM HEPES, 1% penicillin/streptomycin and 4% BSA) containing 1.5 mg/mL of collagenase type I (Millipore-Sigma) for 30 minutes at 37°C. At the end of digestion, 10% FBS was added to stop the reaction. The stromal vascular fraction containing the preadipocytes was pelleted by centrifuging once at 1,000 rpm for 5 minutes at room temperature. The supernatant was discarded and fresh growth medium DMEM high glucose, 20% FBS, 1% penicillin/streptomycin and 20 mM HEPES was added. Cells were mixed, filtered through 100 µm strainer and centrifuged again. The supernatant was discarded, and fresh growth medium was added. Cell viability was assessed by counting number of cells stained with trypan blue (>90% viability). After isolation, cells were plated, allowed to recover and proliferate for 5 days. Next, cells were split again (400,000 cells per well in 6 well-plates) and allowed them to reach 100% confluence before beginning adipocyte differentiation. Each sample was derived from pooled SVF of 10 mice, plated in five 6-well plates. For differentiation, cells were incubated in growth media containing 0.5 mM IBMX, 5 µg/mL insulin, 0.25 µM dexamethasone and 0.5µM rosiglitazone for 2 days, then maintained in growth medium supplemented with 5 g/ml insulin and 0.5µM rosiglitazone for 8 additional days. At the end of differentiation, cells were cultured with growth medium only for 24 hours, then washed

with PBS and incubated in DMEM-high glucose containing 10% exosome-free FBS and 1% penicillin/streptomycin for 48 h for sEV isolation as described below.

**Primary hepatocyte isolation**—Wild-type C57Bl/6J male mice (8–10 weeks old) were purchased from Jackson mice (reference 00664) and anesthetized with avertin. The liver was perfused through the inferior vena cava with PBS-0.5 mM EDTA at a rate of 5 mL/min for 4 minutes followed by a solution of 1.2 mg/mL collagenase type I (ThermoFisher) in DMEM high glucose medium at 5 mL/min for 8 min. The portal vein was cut to allow exit of the solution. Liver pieces were then shaken in a Petri dish to collect released cells. Hepatocytes were pelleted by centrifuging twice in FBS-containing DMEM high glucose at 50 g for 90 sec and filtered through a 100 µm strainer. Cell viability was assessed by counting number of cells stained with trypan blue (>90% viability). One million live cells/well were seeded in collagen pre-coated [overnight, 4°C in collagen from calf skin (Millipore-Sigma)] in four to five 6-well plates per sample. Each sample was derived from the liver of one mouse. The next day, cells were washed and incubated in DMEM-high glucose containing 10% exosome-free FBS and 1% penicillin/streptomycin for 48 hours for sEV isolation as described below.

**Small extracellular vesicle (sEV) isolation**—Blood was obtained from mice by cardiac puncture, let sit in microtainer SST tubes (BD) for 30 min to allow blood coagulation prior to centrifuging at 12,000 g for 5 min at room temperature. Serum was directly processed for sEV isolation as described below. All cell lines were grown to full confluence and differentiated as described above. To collect sEV, cells were washed with PBS and incubated for 48 hours in exosome-free medium [DMEM-High Glucose (ThermoFisher), 10% exosome-free medium (System Biosciences) and 1% Pen/Strep (ThermoFisher)]. Medium was collected and sEV were isolated by differential centrifugation protocol (They et al., 2006). Briefly, medium was successively centrifuged at 500 g, 4,000 g, and 10,000 g for 10 min. In the case of serum, samples were diluted 4 times with 0.22 µm double-filtered PBS and centrifuged at 10,000 g for 10 min. In both serum- and cell-derived samples, supernatant from the 10,000 g spin was later filtered (0.22 µm) and ultracentrifuged at 100,000 g for 70 min using a SW-28 rotor. Pellets were washed with PBS and centrifuged again at 100,000 g for additional 70 min. Pellets (p100) were resuspended in PBS and subjected either to the TMT-Mass spectrometry procedure, nanoparticle tracking analysis or protein isolation procedure for immunoblotting. Similarly, cells that produced the sEV were washed with PBS after the incubation in exosome-free medium and subjected to protein extraction using RIPA lysis buffer (Millipore-Sigma) for immunoblotting.

For some experiments, sEV samples were subjected to an additional isolation step using size exclusion chromatography (SEC). Briefly, the sEV pellet obtained after the second ultracentrifugation at 100,000 g (p100 pellet) was resuspended in 0.5 mL PBS and loaded onto a resin column (qEV 70 nm pore size, polysaccharide resin, iZON). The flow-through was collected in 30 fractions of mL each. An aliquot of each fraction was used for particle concentration determination by nanoparticle tracking analysis (NTA). For protein determination, some fractions were pooled and concentrated using Amicon centrifugal filters (>3 KDa, Millipore-Sigma), as initial protein concentrations were low. All samples

were also subjected to immunoblotting for CD63 and CD9. Two peaks of protein were identified: one, the sEV-SEC, corresponded to fractions 7–10, where most of the vesicles were identified by NTA and samples were positive for CD63 and CD9; and the other, the non-vesicular (NV-SEC) from fractions 17 to 24 having no vesicles by NTA and no CD63/CD9 signal by immunoblotting. For the proteomic study, new freshly prepared sEV-p100 and sEV-SEC samples were isolated. sEV-SEC fractions were concentrated using Amicon 100K centrifugal units (Millipore-Sigma), and both type of samples (sEV-p100 and sEV-SEC) were subjected to mass spectrometry as described below.

### Quantitative mass spectrometry analysis

#### a) Comparative analysis of the sEV proteome from five cell types: 3T3-L1, AML12, C2C12, SVEC and BrAd

*a.1) Sample preparation:* Samples were prepared as previously described (Weekes et al., 2014) with some modifications. sEV were lysed in 8 M Urea, 1% SDS, 50 mM Tris pH 8.5 with cOmplete Protease and PhosStop Phosphatase inhibitor cocktail tablets (Roche) and protein content was measured by micro-BCA assay (ThermoFisher). Proteins were reduced and alkylated as previously described (Weekes et al., 2014). Protein was precipitated using methanol/chloroform. Four volumes of methanol were added to lysate, followed by one volume of chloroform, and three volumes of water. The mixture was vortexed and centrifuged to separate the chloroform phase from the aqueous phase. The precipitated protein pellet was washed with one volume of ice-cold methanol and allowed to air dry. Precipitated proteins were resuspended in 4 M Urea, 50 mM Tris pH 8.5. Proteins were first digested with LysC (1:50; enzyme:protein, Wako) for 12 hours at 25°C.

Samples were diluted in 1 M Urea and 50 mM Tris pH 8.5 and digested with trypsin (1:100; enzyme:protein, ThermoFisher) for another 8 hours at 37°C. Peptides were desalted using a C18 solid phase extraction cartridges as previously described (Weekes et al., 2014). Dried peptides were resuspended in 200 mM EPPS, pH 8.0. Peptide quantification was performed using the micro-BCA assay (Pierce). 50 µg of peptide from each sample was labeled with tandem mass tag (TMT10) reagents (1:4; peptide:TMT label) (Thermo Fisher) for 2 hours at 25°C. Modification of tyrosine residue with TMT was reversed by the addition of 5% hydroxyl amine for 15 minutes at 25°C. The reaction was quenched with 0.5% TFA and a small aliquot of equal volumes of each sample was combined to serve as an internal standard and to check for TMT labeling efficiency and total signal to noise per channel. Final samples were combined to equalize total TMT signal to noise across all channels and desalted on a C18 solid phase extraction cartridge.

*a.2) Liquid chromatography-MS3 spectrometry (LC-MS/MS):* TMT10 multiplexed samples were analyzed with an LC-MS3 data collection strategy (McAlister et al., 2014) on an Orbitrap Fusion mass spectrometer (Thermo Fisher Scientific) equipped with a Proxeon Easy nLC 1000 for online sample handling and peptide separations. Approximately 5 µg of peptide resuspended in 5% formic acid +5% acetonitrile was loaded onto a 100 µm inner diameter fused-silica micro capillary with a needle tip pulled to an internal diameter less than 5 µm. The column was packed in-house to a length of 35 cm with a C18 reverse phase resin (GP118 resin 1.8 µm, 120 Å, Sepax Technologies). The peptides were separated

using a 180 min linear gradient from 3% to 25% buffer B (100% ACN + 0.125% formic acid) equilibrated with buffer A (3% ACN + 0.125% formic acid) at a flow rate of 600 nL/min across the column. The scan sequence for the Fusion Orbitrap began with an MS1 spectrum (Orbitrap analysis, resolution 120,000, 400–1400 m/z scan range, AGC target  $2 \times 10^6$ , maximum injection time 100 ms, dynamic exclusion of 90 seconds). The “Top10” precursors were selected for MS2 analysis, which consisted of CID (quadrupole isolation set at 0.5 Da and ion trap analysis, AGC  $8 \times 10^3$ , NCE 35, maximum injection time 150 ms). The top ten precursors from each MS2 scan were selected for MS3 analysis (synchronous precursor selection), in which precursors were fragmented by HCD prior to Orbitrap analysis (NCE 55, max AGC  $1.5 \times 10^5$ , maximum injection time 150 ms, isolation window 2.5 Da, resolution 60,000).

Because we had 27 samples in total, we equally distributed them based on their source for each 10-plex. For each 10-plex, we chose two control mouse serum sEV, two AdicerKO serum sEV and one sample for each of the five cell lines sEV ( $n = 9$ ). To be able to combine and analyze the data from three different 10-plexes, we used a mix of all our 27 samples and ran it in all  $3 \times 10$ plexes.

## **b) Analysis sEV proteome to compare primary vs immortalized cells and UC vs UC+SEC**

**b.1) Sample preparation:** Exosome samples were reduced with 5 mM DTT for 30 min, alkylated with 10 mM Iodoacetamide for 30 minutes in the dark and quenched with 10 mM DTT for 15 mins. Protein was TCA-precipitated prior to protease digestion. The pellet was re-suspended in 200 mM EPPS, 8 M Urea (pH 8.0) by vortexing. The samples were digested by shaking overnight at room temperature with Lys-C protease at a 50:1 protein-to-protease ratio. Trypsin was then added at a 50:1 protein-to-protease ratio, and the reaction was incubated on a shaker for 6 h at 37°C. The digestion process was quenched with TFA. Acidified digested peptide were desalted over C18 stage tip following protocol described before (Ong et al., 2002).

Six dried, desalted peptides samples were reconstituted with 200 mM EPPS buffer, pH 8.0 and labeled with their respective first 13 of the 16-plex tandem mass tag (TMTPro) reagent. The labeling reactions were performed for 1 hour at room temperature. Modification of tyrosine residues with TMT was reversed by the addition of 5% hydroxyl amine for 15 min, and the reaction was quenched with 0.5% TFA. Samples were combined, further desalted over stage-tip, eluted into an Autosampler Inserts (Thermo Scientific), dried in a speedvac, and reconstituted with 5% acetonitrile-5% TFA for MS analysis.

**b.2) Liquid chromatography-MS2 spectrometry (LC-MS/MS):** A labeled peptide sample from previous step was analyzed with an LC-MS2 data collection strategy on an Orbitrap Fusion Lumos Tribird mass spectrometer (Thermo Fisher Scientific) equipped with a Thermo Easy-nLC 1200 for online sample handling and peptide separations. Resuspended peptide samples were loaded onto a 100  $\mu\text{m}$  inner diameter fused-silica micro capillary with a needle tip pulled to an internal diameter less than 5  $\mu\text{m}$ . The column was packed in-house to a length of 35 cm with a C18 reverse phase resin (GP118 resin 1.8  $\mu\text{m}$ , 120

Å, Sepax Technologies). The peptides were separated using a 180 min linear gradient from 5% to 32% buffer B (90% ACN + 0.1% formic acid) equilibrated with buffer A (5% ACN + 0.1% formic acid) at a flow rate of 550 nL/min across the column. The scan sequence for the Fusion Lumos Orbitrap began with an MS1 spectrum (Orbitrap analysis, resolution 120,000, 400 – 1500 m/z scan range, 250% normalized AGC target, maximum injection time 60 ms, dynamic exclusion of 180 seconds). The instrument was operated in “Top Speed” mode with 3 second cycle time, selecting precursors for HCD MS2 analysis in the orbitrap, with quadrupole isolation set at 0.5 Da, normalized AGC 250%, Collision Energy 35%, maximum injection time 150 ms, resolution 50,000).

For these proteomic studies, we had 12 sEV samples (two biological replicates for each condition) derived from primary vs immortalized cells and sEV isolated by differential ultracentrifugation vs differential ultracentrifugation combined with size exclusion column. A mix of all the samples was added as one sample to each plex and used to normalize the data. In total we had 13 samples and a single 16-plex was enough to perform the experiment.

**c) Mass spectrometry data analysis:** A suite of in-house software tools was used to for .RAW file processing and controlling peptide and protein level false discovery rates, assembling proteins from peptides, and protein quantification from peptides as previously described (Li et al., 2020). Peptide spectral matches were filtered to a 1% false discovery rate (FDR) using the target-decoy strategy combined with linear discriminant analysis. MS/MS spectra were searched against a Uniprot Mouse database with both the forward and reverse sequences. Database search criteria are as follows: tryptic with two missed cleavages, a precursor mass tolerance of 50 ppm, fragment bin tolerance of 0.02, static alkylation of cysteine (57.02146 Da), static TMT labeling of lysine residues and N-termini of peptides (304.2071 Da), and variable oxidation of methionine (15.99491 Da). TMT reporter ion intensities were measured using a 0.003 Da window around the theoretical m/z for each reporter ion. Proteins with <200 summed signal-to-noise across all channels and <0.5 precursor isolation specificity were excluded from the final dataset. The proteins were filtered to a <1% FDR.

**Immunoblotting**—sEV and cells were resuspended in RIPA lysis buffer (Millipore-Sigma) and incubated on ice for 20 min prior to centrifugation at 12,000 *g* for 10 min. Supernatants were used for western blotting in SDS-PAGE electrophoresis. Protein concentration was determined by a BCA kit (ThermoFisher). The following antibodies were used: ADIPOQ (AB3269P, Millipore-Sigma), CD36 (ab133625, Abcam), HSP90alpha (PA3-013, ThermoFisher), POSTN (ab14041, Abcam), PGAM1/4 (sc-376638, Santa Cruz); THBS1 (14778, Cell Signaling), ITGB1 (4706, Cell Signaling), EGFR (2232, Cell Signaling), SPARC (8725, Cell Signaling), IGFBP5 (AF578, R&D systems), CD9 (ab92726, Abcam), CD63 (ab68418, Abcam), CANX (ab22595, Abcam) and FASN (ab22759, Abcam). Given the large difference in the abundance for some of the proteins among different cell types, some of the blots were overexposed to show the signal in as many cell types as possible. Because of this, in some cases, the signal is beyond the linear range, and thus the quantification might not be absolutely accurate. Band intensity quantification was performed using ImageJ software (NIH).

**Adiponectin enzyme-linked immunosorbent assay (ELISA)**—Serum from 12-week-old AdicerKO and control mice were isolated as described above with some modifications. Briefly after serum isolation by using microtainer SST tubes, an aliquot of serum was separated and frozen (serum samples). The rest proceeded to PBS dilution and centrifugation at 10,000 g for 10 min. The supernatant was filtered with 0.22  $\mu\text{m}$  filter and centrifuged at 100,000 g for 70 min. The supernatant was concentrated by using two Amicon Ultra-15 Centrifugal Filter Unit 3K columns per sample (Millipore-Sigma) and centrifuging at 4,000 g for 1 h at 4°C prior to freezing (sEV-free serum samples; approx. final volume was 500  $\mu\text{L}$  from both filters together). Pellets from the 100,000 g centrifugations were resuspended in 400  $\mu\text{L}$  PBS and frozen (sEV samples). For the adiponectin ELISA, we used a total adiponectin ALPCO ELISA kit (catalog nr. 47-ADPMS-E01) and followed manufacturer's instructions. All samples were subjected to protein determination by BCA assay (ThermoFisher). Serum samples required 1/100 dilution for the adiponectin ELISA. Aliquots from sEV-free samples containing the same amount of protein than serum samples were prepared and diluted similarly 1/100 prior the ELISA assay. In the case of sEV, samples were incubated with RIPA lysis buffer for 30 min on ice to open up vesicles and run BCA assay, and 50  $\mu\text{L}$  were used for the ELISA. For the calculations, adiponectin values were normalized by the protein content measured by BCA assay.

**Nanoparticle tracking analysis**—EV concentration and size distribution was determined by the dynamic light scattering technology in a Nanosight LM10 (Malvern Panalytical) at the Nanosight Nanoparticle Sizing & Quantification Facility at Massachusetts General Hospital (Charlestown, MA). The script was programmed to take 4 videos for 30 s each for every sample. The final size and concentrations were determined as the average of the 4 quantifications.

**Electron microscopy**—sEV preparations resuspended in PBS were kept on ice without freezing and submitted to the Electron Microscopy Facility at Harvard Medical School (Boston, MA). For the negative staining of the vesicles, 5  $\mu\text{L}$  of the sample was adsorbed for 1 minute to a formvar/carbon coated grid. Excess liquid was blotted off with a filter paper (Whatman #1), floated on a drop of water to wash away phosphate or salt, blotted again on a filter paper and stained with 0.75% uranyl formate for 30 seconds. After removing the excess uranyl formate with a filter paper, the grids were examined in a JEOL 1200EX transmission electron microscope and images were recorded with an AMT 2k CCD camera. For the CD63 and adiponectin immunostaining, 5  $\mu\text{L}$  of the sample was adsorbed to a carbon coated grid. After blocking with a 1% bovine serum albumin (BSA) solution, grids were incubated with a primary antibody against CD63 (BioLegend 143901, 1:20 dilution) and adiponectin (AB3269P, Millipore-Sigma, 1:40 dilution) for 30 min, washed, and later incubated with a rabbit anti-mouse bridging antibody in 1% BSA (Abcam ab6709, 1:50 dilution) for 20 min. After another wash, grids were incubated with a Protein-A gold 10 nm in 1% BSA (University Medical Center Utrecht, the Netherlands, 1:50 dilution) for 20 min prior to more washing steps. Samples were stained afterwards with 0.75% uranyl formate and examined as the negative staining described above.

**Proteinase treatment**—Serum sEV were resuspended in PBS, treated with either 100 µg/mL of recombinant, PCR grade, Proteinase K (Millipore-Sigma), 0.5% v/v Triton-X100, or both for 15 minutes on ice. After treatment, all samples were incubated with 1mM PMSF proteinase inhibitor (Biotool) for 15 minutes, before undergoing western blotting protocol.

## QUANTIFICATION AND STATISTICAL ANALYSIS

For experiments using cell lines, biological replicates were considered cells growing and being treated/differentiated in different plates and their released exosomes/sEV isolated in different tubes and analyzed separately. In addition, many experimental procedures were performed, and the different biological replicates were collected on separate days or at different times of the day to assure reproducibility of results.

For the analysis of the TMT-Mass Spectrometry results of mouse- and the five cell type-derived sEV (3T3-L1, AML12, C2C12, SVEC and BrAd), each 10-plex consists of 9 samples (2 control mouse serum sEV, 2 AdicerKO serum sEV, and one sEV samples derived from each of the five cell types) and a bridge channel created by pooling material from all 27 experimental samples to be used for normalization across 10-plexes. From the initial 431 proteins identified, 82 were filtered out as not being found in at least two of the three replicates, leading to a total number of 349 different sEV proteins. To discover differential sEV protein expression, we used Limma, an R package for linear modeling that powers differential expression analyses (Ritchie et al., 2006), and a false discovery rate (FDR) < 0.25 (cells *in vitro*) and FDR < 0.05 (mouse data). For the cell types, bar graphs were normalized to the 3T3-L1 value as 1. For the TMT-Mass Spectrometry of primary cells-sEV and SEC-derived sEV, we used a single 16-plex filled with: 2 × 3T3-L1 UC sEV, 2 × 3T3-L1 UC+SEC, 2 × AML12 UC sEV, 2 × AML12 UC+SEC sEV, 2 × primary adipocytes UC sEV, 2 × primary hepatocytes UC sEV and a mixed sample by pooling all these 12 samples for normalization. For the pathway analysis, peptides were annotated to the MSigDB database (UCSD, San Diego, CA; Broad Institute, Cambridge, MA) and compared to our whole dataset as background by Gene Ontology (GO) cellular component (CC) and biological process (BP). Repetitive terms were filtered out of the GO analyses. To identify proteins similarly abundant in sEV from all cell types, the peptides with smallest variance of expression between cell types were selected. The subcellular protein location was extracted from Compartments database (Binder et al., 2014) with a confidence 4. Statistical analysis of comparisons between more than two groups was performed using One-way Analysis of Variance (ANOVA) followed by Bonferroni post hoc T-test.

## Supplementary Material

Refer to Web version on PubMed Central for supplementary material.

## ACKNOWLEDGMENTS

This work was supported by NIH grants R01DK082659 (to C.R.K.), NIDDK 1K01DK117967-01 (to E.A.), and G. Harold & Leila Y. Mathers Foundation grants (to E.A.). R.G.-M. was supported by a Deutsche Forschungsgemeinschaft fellowship (GA 2426/1-1, Germany). We also received support from the Joslin Diabetes Research Center DRC (P30DK036836). We thank Jonathan M. Dreyfuss and Hui Pan from the Joslin Diabetes Center DRC Genomics and Bioinformatics Core for assistance with the data analysis. We also would like to acknowledge Rachel Beth Rodriguez, Ryan Kunz, Mark Jedrychowski, and Julian Mintseris (Harvard Medical

School) for their proteomics services and Steven Gygi (Harvard Medical School) for his support in the proteomic data analysis. The graphical abstract and Figure 1A were created with [BioRender.com](https://BioRender.com)

## REFERENCES

- Andreu Z, and Yanez-Mo M (2014). Tetraspanins in extracellular vesicle formation and function. *Front. Immunol* 5, 442. [PubMed: 25278937]
- Angulski AB, Capriglione LG, Batista M, Marcon BH, Senegaglia AC, Stimamiglio MA, and Correa A (2017). The protein content of extracellular vesicles derived from expanded human umbilical cord blood-derived CD133(+) and human bone marrow-derived mesenchymal stem cells partially explains why both sources are advantageous for regenerative medicine. *Stem Cell Rev. Rep* 13, 244–257. [PubMed: 28054239]
- Arner E, Forrest AR, Ehrlund A, Mejhert N, Itoh M, Kawaji H, Lassmann T, Laurencikiene J, Ryden M, Arner P, et al. (2014). Ceruloplasmin is a novel adipokine which is overexpressed in adipose tissue of obese subjects and in obesity-associated cancer cells. *PLoS One* 9, e80274. [PubMed: 24676332]
- Binder JX, Pletscher-Frankild S, Tsafou K, Stolte C, O'Donoghue SI, Schneider R, and Jensen LJ (2014). Compartments: unification and visualization of protein subcellular localization evidence. *Database (Oxford)* 2014, bau012. [PubMed: 24573882]
- Brandao BB, Madsen S, Rabiee A, Oliverio M, Ruiz GP, Ferrucci DL, Branquinho JL, Razolli D, Pinto S, Nielsen TS, et al. (2020). Dynamic changes in DICER levels in adipose tissue control metabolic adaptations to exercise. *Proc. Natl. Acad. Sci. U S A* 117, 23932–23941. [PubMed: 32900951]
- Crewe C, Joffin N, Rutkowski JM, Kim M, Zhang F, Towler DA, Gordillo R, and Scherer PE (2018). An endothelial-to-adipocyte extracellular vesicle Axis governed by metabolic state. *Cell* 175, 695–708.e3. [PubMed: 30293865]
- Deng ZB, Poliakov A, Hardy RW, Clements R, Liu C, Liu Y, Wang J, Xiang X, Zhang S, Zhuang X, et al. (2009). Adipose tissue exosome-like vesicles mediate activation of macrophage-induced insulin resistance. *Diabetes* 58, 2498–2505. [PubMed: 19675137]
- Durcin M, Fleury A, Taillebois E, Hilairet G, Krupova Z, Henry C, Truchet S, Trötz Müller M, Köfeler H, Mabileau G, et al. (2017). Characterisation of adipocyte-derived extracellular vesicle subtypes identifies distinct protein and lipid signatures for large and small extracellular vesicles. *Journal of Extracellular Vesicles* 10, 1305677.
- Eguchi A, Lasic M, Armando AM, Phillips SA, Katebian R, Maraka S, Quehenberger O, Sears DD, and Feldstein AE (2016). Circulating adipocyte-derived extracellular vesicles are novel markers of metabolic stress. *J. Mol. Med* 94, 1241–1253. [PubMed: 27394413]
- Eguchi J, Wang X, Yu S, Kershaw EE, Chiu PC, Dushay J, Estall JL, Klein U, Maratos-Flier E, and Rosen ED (2011). Transcriptional control of adipose lipid handling by IRF4. *Cell Metab* 13, 249–259. [PubMed: 21356515]
- Escola JM, Kleijmeer MJ, Stoorvogel W, Griffith JM, Yoshie O, and Geuze HJ (1998). Selective enrichment of tetraspan proteins on the internal vesicles of multivesicular endosomes and on exosomes secreted by human B-lymphocytes. *J. Biol. Chem* 273, 20121–20127. [PubMed: 9685355]
- Fasshauer M, Klein J, Ueki K, Kriauciunas KM, Benito M, White MF, and Kahn CR (2000). Essential role of insulin receptor substrate-2 in insulin stimulation of Glut4 translocation and glucose uptake in brown adipocytes. *J. Biol. Chem* 275, 25494–25501. [PubMed: 10829031]
- Figueredo A, Ibarra JL, Bagazgoitia J, Rodriguez A, Molino AM, Fernandez-Cruz A, and Patino R (1993). Plasma C3d levels and ischemic heart disease in type II diabetes. *Diabetes Care* 16, 445–449. [PubMed: 8432215]
- French KC, Antonyak MA, and Cerione RA (2017). Extracellular vesicle docking at the cellular port: extracellular vesicle binding and uptake. *Semin. Cell Dev. Biol* 67, 48–55. [PubMed: 28104520]
- Gabriel K, Ingram A, Austin R, Kapoor A, Tang D, Majeed F, Qureshi T, and Al-Nedawi K (2013). Regulation of the tumor suppressor PTEN through exosomes: a diagnostic potential for prostate cancer. *PLoS One* 8, e70047. [PubMed: 23936141]

- Garcia-Martin R, Wang G, Brandao BB, Zanutto TM, Shah S, Patel S, Schilling B, and Kahn CR (2021). MicroRNA sequence codes for small extracellular vesicle release and cellular retention. *Nature* 10.1038/s41586-021-04234-3.
- Hitosugi T, Zhou L, Elf S, Fan J, Kang HB, Seo JH, Shan C, Dai Q, Zhang L, Xie J, et al. (2012). Phosphoglycerate mutase 1 coordinates glycolysis and biosynthesis to promote tumor growth. *Cancer Cell* 22, 585–600. [PubMed: 23153533]
- Hoshino A, Costa-Silva B, Shen TL, Rodrigues G, Hashimoto A, Tesic Mark M, Molina H, Kohsaka S, Di Giannatale A, Ceder S, et al. (2015). Tumour exosome integrins determine organotropic metastasis. *Nature* 527, 329–335. [PubMed: 26524530]
- Hoshino A, Kim HS, Bojmar L, Gyan KE, Cioffi M, Hernandez J, Zambirinis CP, Rodrigues G, Molina H, Heissel S, et al. (2020). Extracellular vesicle and particle biomarkers define multiple human cancers. *Cell* 182, 1044–1061.e8. [PubMed: 32795414]
- Jeppesen DK, Fenix AM, Franklin JL, Higginbotham JN, Zhang Q, Zimmerman LJ, Liebler DC, Ping J, Liu Q, Evans R, et al. (2019). Reassessment of exosome composition. *Cell* 177, 428–445 e8. [PubMed: 30951670]
- Kalluri R, and LeBleu VS (2020). The biology, function, and biomedical applications of exosomes. *Science* 367, eaau6977. [PubMed: 32029601]
- Kalra H, Drummen GP, and Mathivanan S (2016). Focus on extracellular vesicles: introducing the next small big thing. *Int. J. Mol. Sci* 17, 170. [PubMed: 26861301]
- Kowal J, Arras G, Colombo M, Jouve M, Morath JP, Primdal-Bengtson B, Dingli F, Loew D, Tkach M, and Thery C (2016). Proteomic comparison defines novel markers to characterize heterogeneous populations of extracellular vesicle subtypes. *Proc. Natl. Acad. Sci. U S A* 113, E968–E977. [PubMed: 26858453]
- Kugeratski FG, Hodge K, Lilla S, McAndrews KM, Zhou X, Hwang RF, Zanivan S, and Kalluri R (2021). Quantitative proteomics identifies the core proteome of exosomes with syntenin-1 as the highest abundant protein and a putative universal biomarker. *Nat. Cell Biol* 23, 631–641. [PubMed: 34108659]
- Law RH, Zhang Q, McGowan S, Buckle AM, Silverman GA, Wong W, Rosado CJ, Langendorf CG, Pike RN, Bird PI, et al. (2006). An overview of the serpin superfamily. *Genome Biol* 7, 216. [PubMed: 16737556]
- Li J, Van Vranken, Pontano Vaites L, Schweppe DK, Huttlin EL, Etienne C, Nandhikonda P, Viner R, Robitaille AM, Thompson AH, et al. (2020). TMTpro reagents: a set of isobaric labeling mass tags enables simultaneous proteome-wide measurements across 16 samples. *Nature methods* 17, 399–404. [PubMed: 32203386]
- Logozzi M, Angelini DF, Iessi E, Mizzi D, Di Raimo R, Federici C, Lugini L, Borsellino G, Gentilucci A, Pierella F, et al. (2017). Increased PSA expression on prostate cancer exosomes in vitro condition and in cancer patients. *Cancer Lett* 403, 318–329. [PubMed: 28694142]
- Maffei M, Barone I, Scabia G, and Santini F (2016). The multifaceted haptoglobin in the context of adipose tissue and metabolism. *Endocr. Rev* 37, 403–416. [PubMed: 27337111]
- Mariscal J, Alonso-Nocelo M, Muinelo-Romay L, Barbazan J, Vieito M, Abalo A, Gomez-Tato A, Maria de Los Angeles CC, Garcia-Caballero T, Rodriguez C, et al. (2016). Molecular profiling of circulating tumour cells identifies Notch1 as a principal regulator in advanced non-small cell lung cancer. *Scientific Rep* 6, 37820.
- Mathieu M, Martin-Jaular L, Lavie G, and Thery C (2019). Specificities of secretion and uptake of exosomes and other extracellular vesicles for cell-to-cell communication. *Nat. Cell Biol* 21, 9–17. [PubMed: 30602770]
- McAlister GC, Nusinow DP, Jedrychowski MP, Wuhr M, Huttlin EL, Erickson BK, Rad R, Haas W, and Gygi SP (2014). MultiNotch MS3 enables accurate, sensitive, and multiplexed detection of differential expression across cancer cell line proteomes. *Anal. Chem* 86, 7150–7158. [PubMed: 24927332]
- Moreno-Gonzalo O, Villarroya-Beltri C, and Sanchez-Madrid F (2014). Post-translational modifications of exosomal proteins. *Front. Immunol* 5, 383. [PubMed: 25157254]

- Mori MA, Ludwig RG, Garcia-Martin R, Brandao BB, and Kahn CR (2019). Extracellular miRNAs: from biomarkers to mediators of physiology and disease. *Cell Metab* 30, 656–673. [PubMed: 31447320]
- Mori MA, Thomou T, Boucher J, Lee KY, Lallukka S, Kim JK, Torriani M, Yki-Jarvinen H, Grinspoon SK, Cypess AM, et al. (2014). Altered miRNA processing disrupts brown/white adipocyte determination and associates with lipodystrophy. *J. Clin. Invest* 124, 3339–3351. [PubMed: 24983316]
- Norseen J, Hosooka T, Hammarstedt A, Yore MM, Kant S, Aryal P, Kiernan UA, Phillips DA, Maruyama H, Kraus BJ, et al. (2012). Retinol-binding protein 4 inhibits insulin signaling in adipocytes by inducing proinflammatory cytokines in macrophages through a c-Jun N-terminal kinase- and toll-like receptor 4-dependent and retinol-independent mechanism. *Mol. Cell Biol* 32, 2010–2019. [PubMed: 22431523]
- Obata Y, Kita S, Koyama Y, Fukuda S, Takeda H, Takahashi M, Fujishima Y, Nagao H, Masuda S, Tanaka Y, et al. (2018). Adiponectin/T-cadherin system enhances exosome biogenesis and decreases cellular ceramides by exosomal release. *JCI Insight* 3, e99680.
- Ong SE, Blagoev B, Kratchmarova I, Kristensen DB, Steen H, Pandey A, and Mann M (2002). Stable isotope labeling by amino acids in cell culture, silac, as a simple and accurate approach to expression proteomics. *Mol. Cell Proteomics* 1, 376–386. [PubMed: 12118079]
- Ouchi N, Parker JL, Lugus JJ, and Walsh K (2011). Adipokines in inflammation and metabolic disease. *Nat. Rev. Immunol* 11, 85–97. [PubMed: 21252989]
- Pajvani UB, Hawkins M, Combs TP, Rajala MW, Doebber T, Berger JP, Wagner JA, Wu M, Knopps A, Xiang AH, et al. (2004). Complex distribution, not absolute amount of adiponectin, correlates with thiazolidinedione-mediated improvement in insulin sensitivity. *J. Biol. Chem* 279, 12152–12162. [PubMed: 14699128]
- Parker-Duffen JL, Nakamura K, Silver M, Kikuchi R, Tigges U, Yoshida S, Denzel MS, Ranscht B, and Walsh K (2013). T-cadherin is essential for adiponectin-mediated revascularization. *J. Biol. Chem* 288, 24886–24897. [PubMed: 23824191]
- Peake PW, Kriketos AD, Campbell LV, Shen Y, and Charlesworth JA (2005). The metabolism of isoforms of human adiponectin: studies in human subjects and in experimental animals. *Eur. J. Endocrinol* 153, 409–417. [PubMed: 16131604]
- Phielier J, Chung KJ, Chatzigeorgiou A, Klotzsche-von Ameln A, Garcia-Martin R, Sprott D, Moissidou M, Tzanavari T, Ludwig B, Baraban E, et al. (2013a). The complement anaphylatoxin C5a receptor contributes to obese adipose tissue inflammation and insulin resistance. *J. Immunol* 191, 4367–4374. [PubMed: 24043887]
- Phielier J, Garcia-Martin R, Lambris JD, and Chavakis T (2013b). The role of the complement system in metabolic organs and metabolic diseases. *Semin. Immunol* 25, 47–53. [PubMed: 23684628]
- Ponka P (1999). Cellular iron metabolism. *Kidney Int. Suppl* 69, S2–S11. [PubMed: 10084280]
- Rajendran L, Honsho M, Zahn TR, Keller P, Geiger KD, Verkade P, and Simons K (2006). Alzheimer's disease beta-amyloid peptides are released in association with exosomes. *Proc. Natl. Acad. Sci. U S A* 103, 11172–11177. [PubMed: 16837572]
- Ritchie ME, Diyagama D, Neilson J, van Laar R, Dobrovic A, Holloway A, and Smyth GK (2006). Empirical array quality weights in the analysis of microarray data. *BMC Bioinformatics* 7, 261. [PubMed: 16712727]
- Saman S, Kim W, Raya M, Visnick Y, Miro S, Saman S, Jackson B, McKee AC, Alvarez VE, Lee NC, et al. (2012). Exosome-associated tau is secreted in tauopathy models and is selectively phosphorylated in cerebrospinal fluid in early Alzheimer disease. *J. Biol. Chem* 287, 3842–3849. [PubMed: 22057275]
- Sano S, Izumi Y, Yamaguchi T, Yamazaki T, Tanaka M, Shiota M, Osada-Oka M, Nakamura Y, Wei M, Wanibuchi H, et al. (2014). Lipid synthesis is promoted by hypoxic adipocyte-derived exosomes in 3T3-L1 cells. *Biochem. Biophys. Res. Commun* 445, 327–333. [PubMed: 24513287]
- Saunderson SC, Schubert PC, Dunn AC, Miller L, Hock BD, MacKay PA, Koch N, Jack RW, and McLellan AD (2008). Induction of exosome release in primary B cells stimulated via CD40 and the IL-4 receptor. *J. Immunol* 180, 8146–8152. [PubMed: 18523279]

- Shapiro L, and Scherer PE (1998). The crystal structure of a complement-1q family protein suggests an evolutionary link to tumor necrosis factor. *Curr. Biol* 8, 335–338. [PubMed: 9512423]
- Shim K, Begum R, Yang C, and Wang H (2020). Complement activation in obesity, insulin resistance, and type 2 diabetes mellitus. *World J. Diabetes* 11, 1–12. [PubMed: 31938469]
- Silverman GA, Bird PI, Carrell RW, Church FC, Coughlin PB, Gettins PG, Irving JA, Lomas DA, Luke CJ, Moyer RW, et al. (2001). The serpins are an expanding superfamily of structurally similar but functionally diverse proteins. Evolution, mechanism of inhibition, novel functions, and a revised nomenclature. *J. Biol. Chem* 276, 33293–33296. [PubMed: 11435447]
- Skog J, Wurdinger T, van RS, Meijer DH, Gainche L, Sena-Esteves M, Curry WT Jr., Carter BS, Krichevsky AM, and Breakefield XO (2008). Glioblastoma microvesicles transport RNA and proteins that promote tumour growth and provide diagnostic biomarkers. *Nat. Cell Biol* 10, 1470–1476. [PubMed: 19011622]
- Smith U, and Kahn BB (2016). Adipose tissue regulates insulin sensitivity: role of adipogenesis, de novo lipogenesis and novel lipids. *J. Intern. Med* 280, 465–475. [PubMed: 27699898]
- Thery C, Amigorena S, Raposo G, and Clayton A (2006). Isolation and characterization of exosomes from cell culture supernatants and biological fluids. *Curr. Protoc. Cell Biol*, Chapter 3, Unit 3 22.
- Thomou T, Mori MA, Dreyfuss JM, Konishi M, Sakaguchi M, Wolfrum C, Rao TN, Winnay JN, Garcia-Martin R, Grinspoon SK, et al. (2017). Adipose-derived circulating miRNAs regulate gene expression in other tissues. *Nature* 542, 450–455. [PubMed: 28199304]
- Valadi H, Ekstrom K, Bossios A, Sjostrand M, Lee JJ, and Lotvall JO (2007). Exosome-mediated transfer of mRNAs and microRNAs is a novel mechanism of genetic exchange between cells. *Nat. Cell Biol* 9, 654–659. [PubMed: 17486113]
- van Niel G, D’Angelo G, and Raposo G (2018). Shedding light on the cell biology of extracellular vesicles. *Nat. Rev. Mol. Cell Biol* 19, 213–228. [PubMed: 29339798]
- Villarroya-Beltri C, Baixauli F, Gutierrez-Vazquez C, Sanchez-Madrid F, and Mittelbrunn M (2014). Sorting it out: regulation of exosome loading. *Semin. Cancer Biol* 28, 3–13. [PubMed: 24769058]
- Weekes MP, Tomasec P, Huttlin EL, Fielding CA, Nusinow D, Stanton RJ, Wang ECY, Aicheler R, Murrell I, Wilkinson GWG, et al. (2014). Quantitative temporal viromics: an approach to investigate host-pathogen interaction. *Cell* 157, 1460–1472. [PubMed: 24906157]
- Wei Z, Batagov AO, Schinelli S, Wang J, Wang Y, El Fatimy R, Rabinovsky R, Balaj L, Chen CC, Hochberg F, et al. (2017). Coding and non-coding landscape of extracellular RNA released by human glioma stem cells. *Nat. Commun* 8, 1145. [PubMed: 29074968]
- Whitham M, Parker BL, Friedrichsen M, Hingst JR, Hjorth M, Hughes WE, Egan CL, Cron L, Watt KI, Kuchel RP, et al. (2018). Extracellular Vesicles Provide a Means for Tissue Crosstalk during Exercise. *Cell Metab* 27, 237–251.e4. [PubMed: 29320704]
- Wu JC, Merlino G, and Fausto N (1994). Establishment and characterization of differentiated, nontransformed hepatocyte cell lines derived from mice transgenic for transforming growth factor alpha. *Proc. Natl. Acad. Sci. U S A* 91, 674–678. [PubMed: 7904757]
- Yaffe D, and Saxel O (1977). Serial passaging and differentiation of myogenic cells isolated from dystrophic mouse muscle. *Nature* 270, 725–727. [PubMed: 563524]
- Yamauchi T, and Kadowaki T (2013). Adiponectin receptor as a key player in healthy longevity and obesity-related diseases. *Cell Metab* 17, 185–196. [PubMed: 23352188]
- Yang JM, and Gould SJ (2013). The cis-acting signals that target proteins to exosomes and microvesicles. *Biochem. Soc. Trans* 41, 277–282. [PubMed: 23356297]
- Yang Q, Graham TE, Mody N, Preitner F, Peroni OD, Zabolotny JM, Kotani K, Quadro L, and Kahn BB (2005). Serum retinol binding protein 4 contributes to insulin resistance in obesity and type 2 diabetes. *Nature* 436, 356–362. [PubMed: 16034410]
- Ying W, Riopel M, Bandyopadhyay G, Dong Y, Birmingham A, Seo JB, Ofrecio JM, Wollam J, Hernandez-Carretero A, Fu W, et al. (2017). Adipose tissue macrophage-derived exosomal miRNAs can modulate in vivo and in vitro insulin sensitivity. *Cell* 171, 372–384 e312. [PubMed: 28942920]
- Yoshida M, Satoh A, Lin JB, Mills KF, Sasaki Y, Rensing N, Wong M, Apte RS, and Imai SI (2019). Extracellular vesicle-contained eNAMPT delays aging and extends lifespan in mice. *Cell Metab* 30, 329–342 e325. [PubMed: 31204283]

- Yoshioka Y, Konishi Y, Kosaka N, Katsuda T, Kato T, and Ochiya T (2013). Comparative marker analysis of extracellular vesicles in different human cancer types. *J. Extracell. Vesicles* 2.
- Zhang Q, Higginbotham JN, Jeppesen DK, Yang YP, Li W, McKinley ET, Graves-Deal R, Ping J, Britain CM, Dorsett KA, et al. (2019). Transfer of functional cargo in exomeres. *Cell Rep* 27, 940–954 e946. [PubMed: 30956133]
- Zhao H, Shang Q, Pan Z, Bai Y, Li Z, Zhang H, Zhang Q, Guo C, Zhang L, and Wang Q (2018). Exosomes from adipose-derived stem cells attenuate adipose inflammation and obesity through polarizing M2 macrophages and beiging in white adipose tissue. *Diabetes* 67, 235–247. [PubMed: 29133512]
- Zhou L, Deepa SS, Etzler JC, Ryu J, Mao X, Fang Q, Liu DD, Torres JM, Jia W, Lechleiter JD, et al. (2009). Adiponectin activates AMP-activated protein kinase in muscle cells via APPL1/LKB1-dependent and phospholipase C/Ca<sup>2+</sup>/Ca<sup>2+</sup>/calmodulin-dependent protein kinase kinase-dependent pathways. *J. Biol. Chem* 284, 22426–22435. [PubMed: 19520843]

### Highlights

- Different cell types release unique patterns of exosomal/sEV proteins
- sEV markers, like tetraspanins, vary in abundance in sEV of different cell types
- *In vitro* sEV proteome can serve to predict tissue-of-origin of circulating sEV *in vivo*
- Adiponectin is an adipose tissue-specific sEV marker

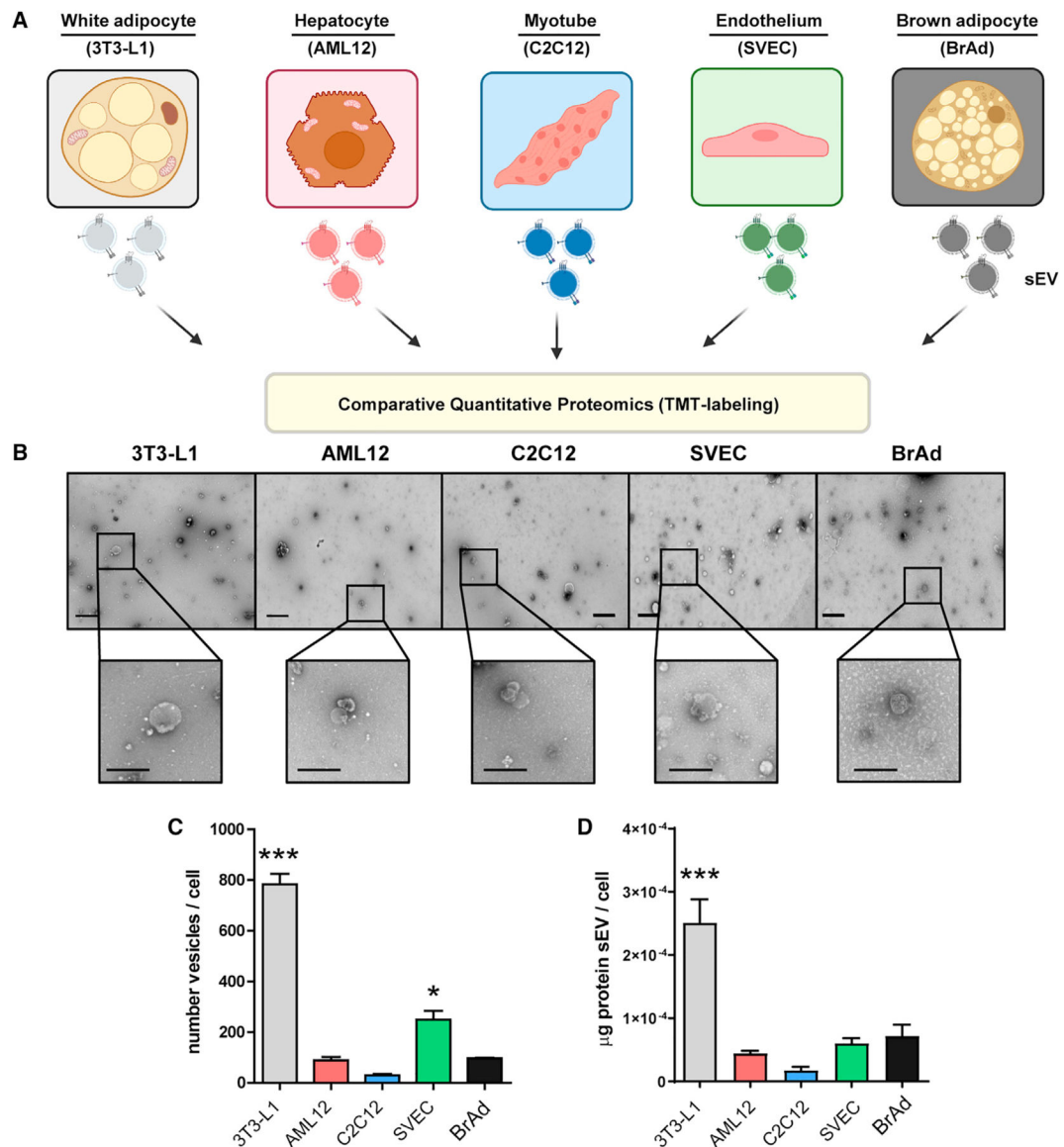


**Figure 1. Experimental design and characterization of sEVs released by each cell type**  
 (A) Diagram representing the experimental model. Differentiated white adipocytes (3T3-L1), differentiated immortalized brown adipocytes (BrAd), differentiated C2C12 myotubes, hepatocytes (AML12), and endothelial cells (SVEC) were cultured in exosome-free medium for 48 h and sEVs were collected by differential centrifugation. Protein was isolated and equal amount from each cell type was subjected to a quantitative proteomics based following TMT labeling.

(B) Representative electron microscopy images from sEVs isolated from each cell type. Scale bar, 500 nm in the low-magnification pictures (larger squares, above) and 200 nm in the higher-magnification pictures (smaller squares, below).

(C) Number of sEVs released by each cell type normalized by the number of cells in the culture plates from which the vesicles were collected. For 3T3-L1 cells, the value corresponds to the average of 4 different clones.

(D) Protein concentration determined by bicinchoninic acid (BCA) of the sEVs released to the culture medium by each cell type and normalized by the number of cells present in the culture plates.

Data are expressed as means  $\pm$  SEMs; n = 4. \*p < 0.05 between indicated cell type and the other 4, \*\*\*p < 0.001 between the indicated cell type and the other 4.

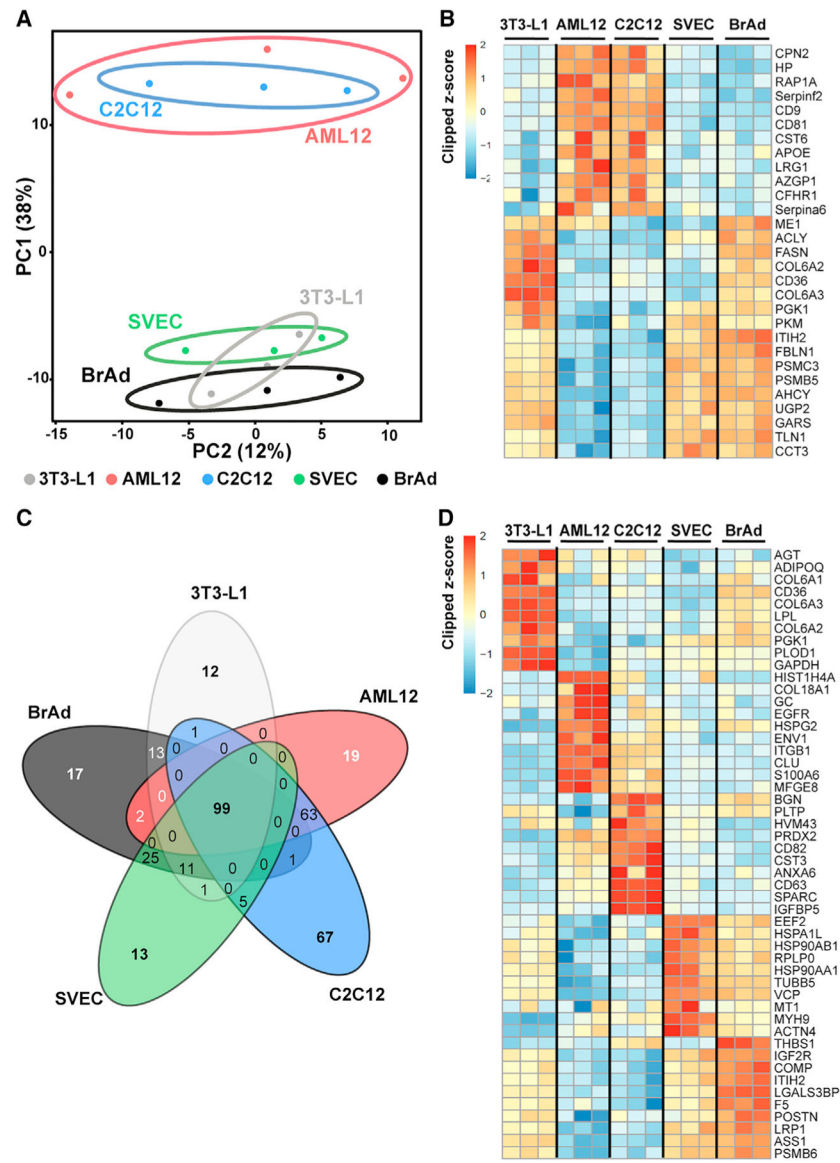


**Figure 2. Proteomic patterns observed in the isolated sEVs**

(A) Principal-component analysis (PCA) of the sEV proteome by each cell type showing 2 distinct clusters: hepatocytes/myotubes and endothelium/white adipocytes/brown adipocytes. This and all of the subsequent figures are based on 3 biological replicates for sEVs of each cell type.

(B) Heatmap showing some proteins characteristic of each cluster found in the PCA depicted in (A): 12 proteins were enriched in sEV derived from AML12 hepatocytes and C2C12 myotubes, 6 proteins were enriched in sEV from 3T3-L1 adipocytes and BrAd, and 11 proteins were significantly enriched in sEV from SVEC endothelial cells, 3T3-L1 white adipocytes, and BrAd brown adipocytes.

(C) Venn diagram showing the number of unique proteins significantly enriched in the sEVs from each cell type and their combinations. The number in the center represents those

proteins present at similar levels in the sEVs from all of the cell types. The total number of unique proteins is 349. FDR < 0.25.

(D) Heatmap showing the top-10 proteins significantly enriched in the sEVs from each cell type in specific.

Author Manuscript

Author Manuscript

Author Manuscript

Author Manuscript

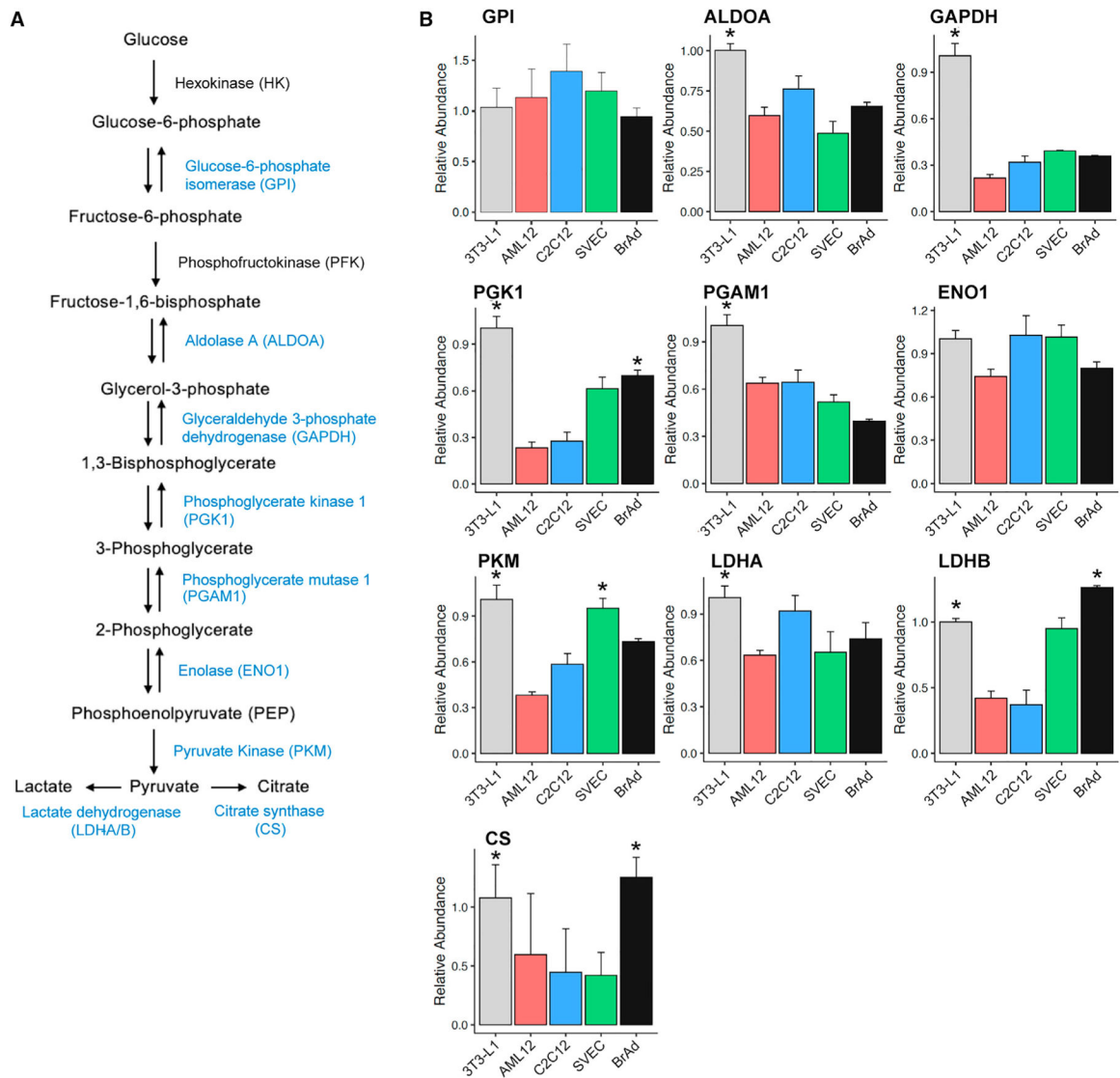


**Figure 3. Glycolytic enzymes are enriched in adipocyte-derived sEVs**

(A) The glycolytic pathway scheme showing the enzymes involved at each step, their substrates, and their products. In blue are the enzymes found in the sEVs in our experiments.

(B) Bar graphs for the sEV relative abundance in the proteomics study in each of the indicated cell types. Data are expressed as means  $\pm$  SEMs. \* $p < 0.05$  versus all other cell types ( $n = 3$ ).

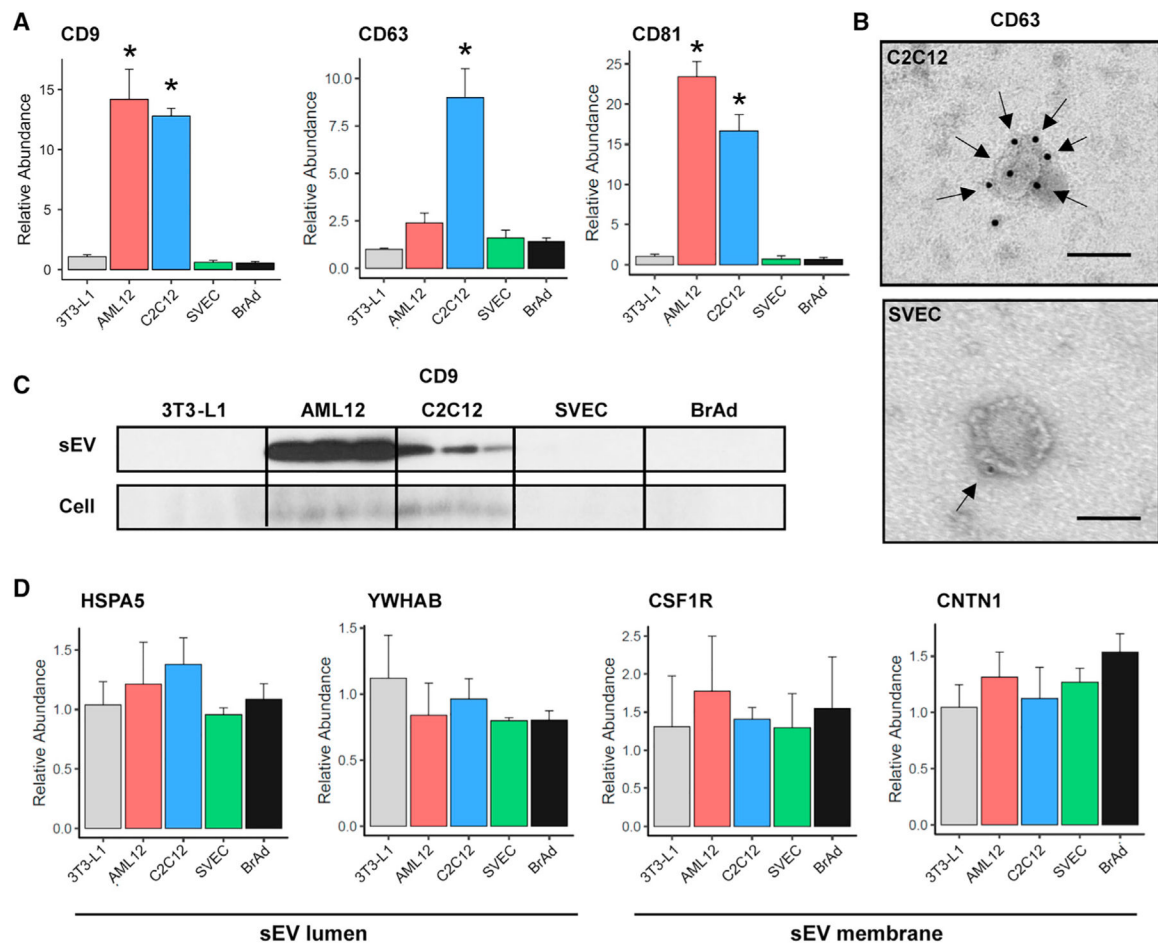


**Figure 4. Tetraspanins are not equally expressed in sEVs from different cell types**

Identification of other potential sEV markers.

(A) Bar graphs for the sEV abundance of CD9 (left), CD63 (center), and CD81 (right) obtained from the proteomics study ( $n = 3$ ).

(B) Representative immunoelectron microscopic images for CD63 of vesicles isolated from C2C12 (up) and SVEC (down). Scale bar, 100 nm. Arrows indicate CD63<sup>+</sup> signal.

(C) Immunoblotting for CD9 in sEVs (upper blot) and cell bodies (lower blot) from the indicated cell types.

(D) Bar graphs for the sEV relative abundance given by the proteomics study in the indicated cell types of heat shock family A member 5 (HSPA5, also known as HSP70 or BiP), 14–3–3 protein beta/alpha (YWHAB), colony-stimulating factor 1 receptor (CSF1R), and contactin-1 (CNTN1).

Data are expressed as means  $\pm$  SEMs.  $n = 3$  for sEV samples and  $n = 4$  for cell samples. \* $p < 0.05$  versus all other cell types.

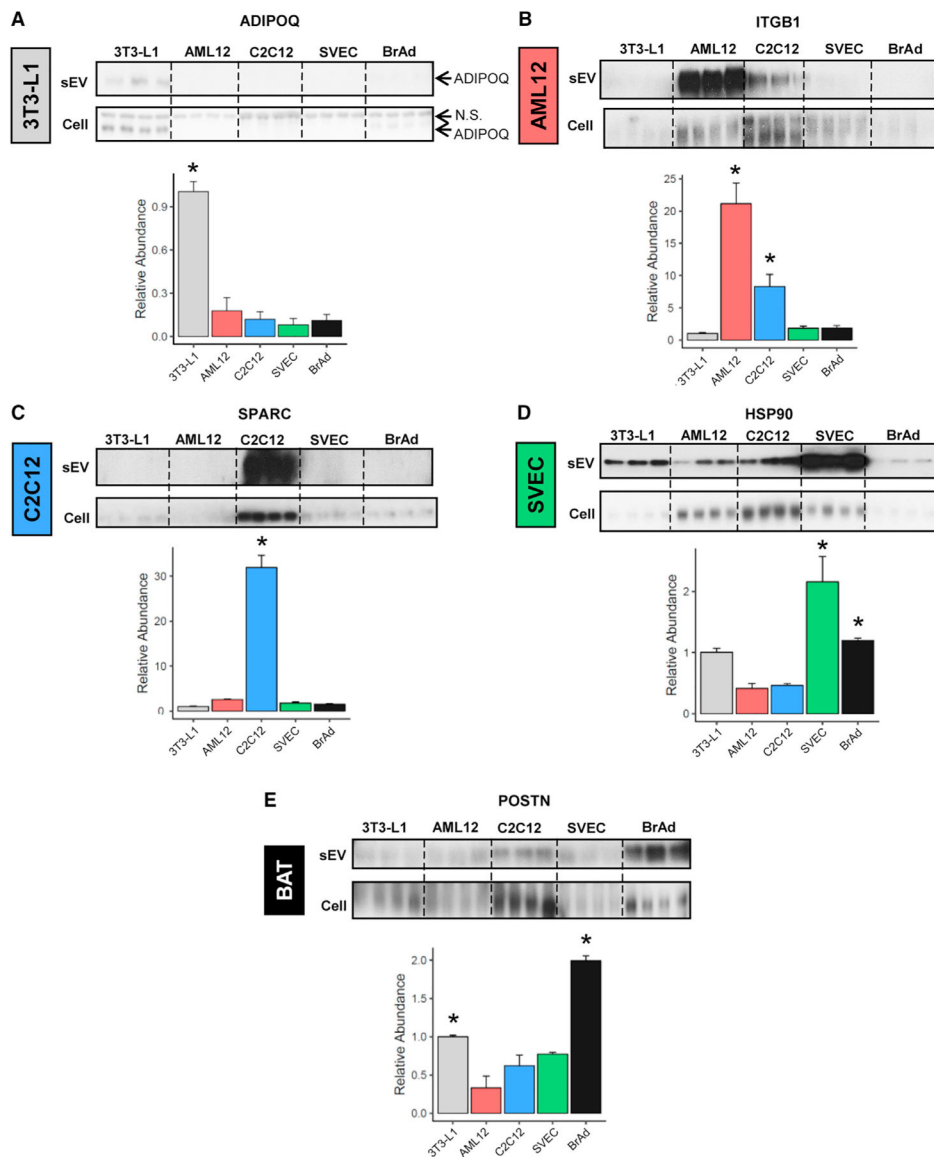


### Figure 5. Immunoblotting of sEV markers for each cell type

Immunoblotting (above) in sEVs (upper panel) and cell bodies (lower panel) and bar graphs from proteomics study (below) from the indicated cell types for adiponectin (ADIPOQ) (A), integrin b1 (ITGB1) (B), secreted protein acidic and cysteine-rich (SPARC) (C), heat shock protein 90AA1 (HSP90) (D), and periostin (POSTN) (E). Data are expressed as means  $\pm$  SEMs. \* $p < 0.05$  versus all other cell types ( $n = 3$  for sEV and  $n = 4$  for cell samples).

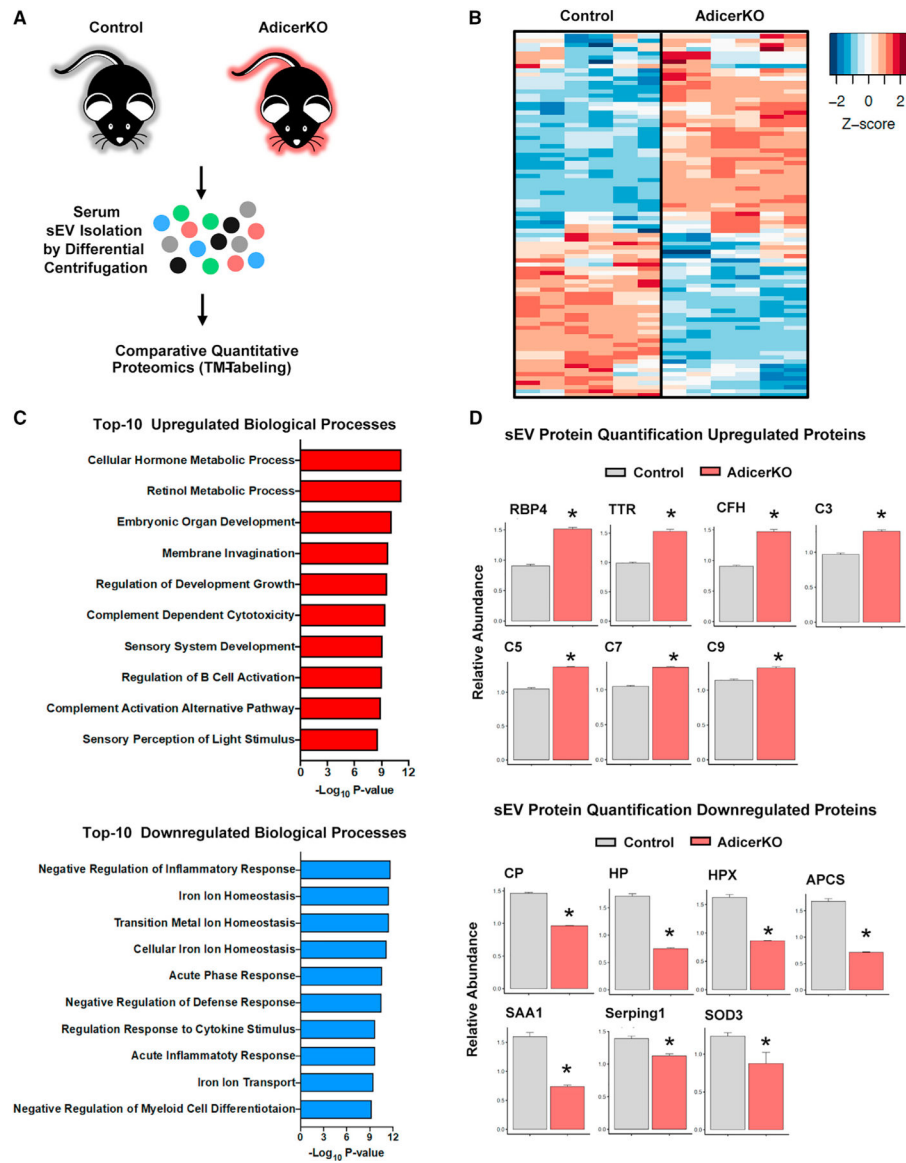


**Figure 6. Changes in serum sEV protein profile in AdicerKO mice**

(A) Diagram representing the experimental model. Serum from random-fed control (ADIPOQ-Cre<sup>-</sup> Dicer<sup>fl/fl</sup>) and adipose tissue-specific Dicer knockout mice (AdicerKO, ADIPOQCre<sup>+</sup> Dicer<sup>fl/fl</sup>) was collected, and sEVs were isolated. Equal amounts of protein of each were then subjected to quantitative proteomics using the TMT-labeling technique.

(B) Heatmap showing the 86 proteins significantly regulated (FDR < 0.05) in the sEVs from AdicerKO versus control.

(C) Top 10 upregulated biological processes determined by Gene Ontology (GO) from the 40 sEV proteins upregulated in the serum from AdicerKO compared to control mice (FDR < 0.01).

(D) Relative abundance by the proteomics assay for selected upregulated proteins in AdicerKO compared to control mice (n = 6).

(E) Top 10 downregulated biological processes from the 46 downregulated sEV proteins determined by GO in the serum from AdicerKO mice compared to control mice (FDR < 0.01).

(F) Relative abundance measured by the proteomics assay of selected downregulated proteins in AdicerKO compared to control mice (n = 6).

Data are expressed as means  $\pm$  SEMs. \*p < 0.05 AdicerKO-versus control-derived sEVs.

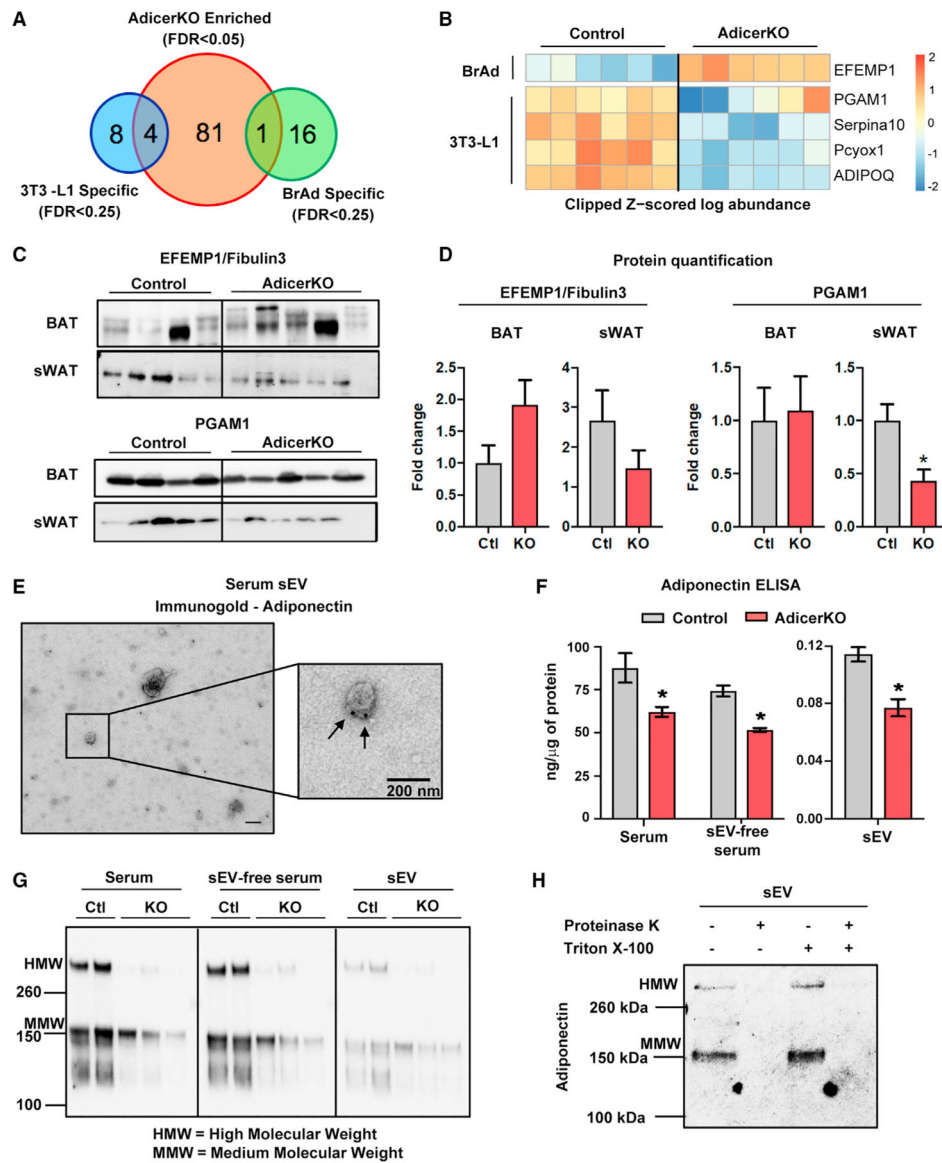


**Figure 7. High-molecular-weight ADIPOQ is downregulated in sEV from AdicerKO mice**

(A) Venn diagram representing the intersection of the 86 differentially regulated sEV proteins from AdicerKO vs control (large circle) with the 12 white adipocyte 3T3-L1 derived (left circle) and 17 BrAd derived (right circle) from our *in vitro* comparative proteomics.

(B) Heatmap showing the protein abundance in sEVs from AdicerKO and control sera for the 5 sEV proteins predicted to be derived from adipocytes.

(C) Western blot for EFEMP1/fibulin-3 (up) and PGAM1 (down) in brown adipose tissue (BAT) (n = 4 for control and 5 for AdicerKO) and subcutaneous inguinal white adipose tissue (sWAT) (n = 5 for control and AdicerKO).

(D) Protein quantification from the blots depicted in (C) (n = 4 for control and n = 5 for AdicerKO for BAT and n = 5 for control and AdicerKO for sWAT).

(E) Representative immunoelectron microscopic images for ADIPOQ in serum sEVs. Scale bar, 200 nm in both pictures.

(F) ADIPOQ levels detected by ELISA in serum, sEV-free serum, and sEVs, from AdicerKO and control mice (n = 5).

(G) ADIPOQ western blot from serum, sEV-free serum, and isolated sEV from control (Ctl) and AdicerKO (KO) mice. HMW indicates high molecular weight ADIPOQ, while MMW refers to medium molecular weight ADIPOQ. Samples were pooled: wild type (WT) n = 2 and AdicerKO n = 3 (3 animals per sample).

(H) sEVs were isolated and left untreated (first lane) or treated with either 100 µg/mL recombinant proteinase K or 0.5% v/v Triton X-100, or both (representative of 2 independent experiments).

SDS gels for experiments shown in (G) and (H) were performed under non-reducing conditions. Ponceau staining was used to normalize the tissue abundance of EFEMP1/fibulin-3 and PGAM1 (Figure S7F). Data are expressed as means ± SEMs. \*p < 0.05 versus all other cell types.

## KEY RESOURCES TABLE

REAGENT or RESOURCE	SOURCE	IDENTIFIER
Antibodies		
Adiponectin	Millipore-Sigma	Cat#: AB3269P; RRID:AB_2273529
CANX	Abcam	Cat#: ab22595; RRID:AB_2069006
CD9	Abcam	Cat#: ab92726; RRID:AB_10561589
CD36	Abcam	Cat#: ab133625; RRID:AB_2716564
CD63 (immunoblotting)	Abcam	Cat#: ab68418; RRID:AB_10563972
CD63 (electromicroscopy)	BioLegend	Cat#: 143901; RRID:AB_11203908
EGFR	Cell Signaling	Cat#: 2232; RRID:AB_331707
FASN	Abcam	Cat#: ab22759; RRID:AB_732316
HSP90alpha	ThermoFisher	Cat#: PA3-013; RRID:AB_2120934
IGFBP5	R&D Systems	Cat#: AF578; RRID:AB_2123485
ITGB1	Cell Signaling	Cat#: 4706; RRID:AB_823544
Periostin	Abcam	Cat#: ab14041; RRID:AB_2299859
Pgam1/4	Santa Cruz	Cat#: sc-376638; RRID:AB_11150476
SPARC	Cell Signaling	Cat#: 8725; RRID:AB_10860770
Thrombospondin-1	Cell Signaling	Cat#: 14778
Goat anti-rabbit IgG (H+L)-HRP conjugate	BioRad	Cat#: 1706515; RRID:AB_11125142
Rabbit Anti-Mouse IgG H&L	Abcam	Cat#: ab6709; RRID:AB_956006
Sheep anti-mouse-HRP conjugate	GE Healthcare	Cat#: NA931V; RRID:AB_772210
Chemicals, peptides, and recombinant proteins		
Avertin (2,2,2-Tribromoethanol)	Millipore-Sigma	Cat#: T48402
Collagenase type-I	ThermoFisher	Cat#: 17100017
Collagen from calf skin	Millipore-Sigma	Cat#: C8919
IBMX (3-Isobutyl-1-methylxanthine)	Millipore-Sigma	Cat#: I5879
Indomethacin	Millipore-Sigma	Cat#: I7378
Insulin	Millipore-Sigma	Cat#: I9278
ITS-A	ThermoFisher	Cat#: 51-300-044
LysC (Lysyl Endopeptidase)	Fujifilm-Wako	Cat#: 125-05061
Rosiglitazone	Millipore-Sigma	Cat#: R2408
T3 [3,3',5-Triiodo-L-thyronine]	Millipore-Sigma	Cat#: T6397
Trypsin	ThermoFisher	Cat#: 90058
Critical commercial assays		
Mouse HMW & Total Adiponectin ELISA	ALPCO	Cat#: 47-ADPMS-E01
Deposited data		
Raw mass spectrometry data	This paper	Accession number PXD030240
Experimental models: Cell lines		

REAGENT or RESOURCE	SOURCE	IDENTIFIER
3T3-L1	ATCC	Cat#: CL-173
AML12	ATCC	Cat#: CRL-2254
C2C12	ATCC	Cat#: CRL-1772
SVEC	ATCC	Cat#: CRL-2181
BAT	Fasshauer et al. (2000)	N/A
Experimental models: Organisms/strains		
Mouse: Adiponectin-Cre Dicer floxed	Mori et al. (2014)	N/A
Mouse: C57BL/6J wild-type	Jackson mice	No. 000664
Software and algorithms		
Excel	Microsoft	N/A
Biorender	<a href="https://biorender.com/">https://biorender.com/</a>	N/A
Gen5 v3.11.19	Biotek	N/A
NTA v3.2	Malvern Panalytical	N/A
GraphPad Prism v8	GraphPad software	N/A
R software v4	R project	N/A
SPSS v20	IBM	N/A
Word	Microsoft	N/A
Other		
Microtainer capillary blood collectors	BD	Cat#: 365967
SW28 rotor	Beckman Coulter	Cat#: 342207
qEVoriginal / 70nm	iZON	SP1
Nanosight LM10	Malvern Panalytical	N/A
Orbitrap Fusion Lumos Tribrid Mass Spectrometer	ThermoFisher	Cat#: IQLAAEGAAPFADBMBHQ
Open-Top Thickwall Polycarbonate Tube	Beckman Coulter	Cat#: 355631
Amicon Ultra-0.5 3K Centrifugal Filter Unit	Millipore-Sigma	Cat#: UFC500324
Amicon Ultra-2 100K Centrifugal Filter Unit	Millipore-Sigma	Cat#: UFC210024